bioRxiv preprint doi: https://doi.org/10.1101/267708; this version posted February 18, 2018. The copyright holder for this preprint (which was not certified by peer review) is the author/funder. All rights reserved. No reuse allowed without permission.

**Noname manuscript No.**
(will be inserted by the editor)

# Spatial moment description of birth-death-movement processes incorporating the effects of crowding and obstacles

**Anudeep Surendran** [1] · **Michael J. Plank** [2,3] · **Matthew J. Simpson** [1]

Received: date / Accepted: date

**Abstract** Birth-death-movement processes, modulated by interactions between individuals, are fundamental to many biological processes such as development, repair and disease. Similar interactions are also relevant in ecology. A key feature of the movement of cells within *in vivo* environments are the interactions between motile cells and stationary obstacles, such as the extracellular matrix and stationary macromolecules. Here we propose a multi-species individual-based model (IBM) of individual-level motility, proliferation and death. In particular, we focus on examining the case where we consider a population of motile, proliferative agents within an environment that is populated by stationary, non-proliferative obstacles. To provide a mathematical foundation for the analysis of the IBM, we derive a system of spatial moment equations that approximately governs the evolution of the density of agents and the density of pairs of agents. By using a spatial moment approach we avoid making the usual mean field assumption so that our IBM and continuous model are able to predict the formation of spatial structure, such as clustering and aggregation. We explore several properties of the obstacle field, such as systematically varying the obstacle density, obstacle size, and the nature and strength of the interactions between the motile, proliferative agents and the stationary, non-proliferative obstacles. Overall we find that the spatial moment model provides a reasonably accurate prediction of the dynamics of the system, including subtle but important effects, such as how varying the properties of the obstacles leads to different patterns of clustering and segregation in the population.

**Keywords** Collective cell migration · Spatial moment dynamics · Individual based model · proliferation · migration · Birth-death process

[1]School of Mathematical Sciences, Queensland University of Technology, Brisbane Queensland, Australia. [2]School of Mathematics and Statistics, University of Canterbury, Christchurch, New Zealand. [3]Te Pūnaha Matatini, A New Zealand Centre of Research Excellence, Auckland, New Zealand.
E-mail: matthew.simpson@qut.edu.au.

bioRxiv preprint doi: https://doi.org/10.1101/267708; this version posted February 18, 2018. The copyright holder for this preprint (which was not certified by peer review) is the author/funder. All rights reserved. No reuse allowed without permission.



## 1 Introduction

Movement, birth and death processes are important individual-level mechanisms that can drive population-level outcomes in both biological and ecological systems. Cell migration and cell proliferation, modulated by interactions among neighboring cells, are essential for embryonic development (Kurosaka and Kashina 2008), tissue repair (Martin 1997; Shaw and Martin 2009) and many diseases, including cancer (Friedl and Wolf 2003). Live cell imaging and simulation-based studies show that the movement of intracellular molecules is also strongly influenced by crowding (Hasnain et al. 2014; Reverey et al. 2015). Similarly, in many ecological systems, the movement of individuals, and interactions between individuals, can have important consequences on the spatio-temporal dynamics of the population. Interspecies spatial segregation and intraspecies clustering in predator-prey systems (Tobin and Bjornstad 2003) and the emergence of spatial structure in plant communities (Law and Dieckmann 2000) are direct results of interactions between individuals. These common observations from different areas of the life sciences suggest a role for individual-level, agent-based mathematical models to represent molecules, cells, plants and animals. Popular modelling frameworks include lattice-based models and continuous space lattice free models (Plank and Simpson 2012; Bruna and Chapman 2012; Dyson and Baker 2015). Some of these models consider the dynamics and interaction within a single population (Lewis 2000; Middleton et al. 2014). Other models, often called multi-species models, directly incorporate the influence of interaction among different types of agents to represent different subpopulations (Murrell 2005; Plank and Law 2015; Smith et al. 2017).

Cell migration in living tissues involves complicated heterogeneous environments that are occupied by various biological structures and scaffolds, including macromolecules and cells of varying size, shape and adhesive properties (Ellery et al. 2014; Ellery et al. 2016). Such obstacles and scaffolds can have a significant impact on the migration of cells due to the interplay between crowding and cell-to-substrate adhesion (Welch 2015; Sun and Zaman 2017; Simpson and Plank 2017). The extracellular matrix (ECM), composed of polysaccharides and protein fibers, is one example of a biological obstacle which influences the cell migration in many different ways, such as providing biochemical stimuli, mechanical cues and steric hindrances (Zaman et al. 2006; Harley et al. 2008). ECM geometry and microarchitecture play a significant role in regulating the motility of cancer (Condeelis and Segall 2003) and immune cells (Bajenoff et al. 2006). The highly compartmentalised structure of the cytoplasm and the presence of macromolecular obstacles such as nucleic acids, proteins and polysaccharides in intracellular environments is known to have a significant impact on both biochemical reactions (Minton 2001; Tan et al. 2013; Hansen et al. 2016) and physical transport processes inside the cell (Ghosh et al. 2016; Smith et al. 2017). These examples from various organizational levels suggest that the incorporation of both obstacles and their crowding effects in a mathematical model of cell migration is important. In

bioRxiv preprint doi: https://doi.org/10.1101/267708; this version posted February 18, 2018. The copyright holder for this preprint (which was not certified by peer review) is the author/funder. All rights reserved. No reuse allowed without permission.



this tudy, we explicitly consider how various properties of the crowding environment, such as obstacle size, density and obstacle adhesion, impacts the population-level dynamics of a population of agents in a discrete individual based model (IBM) of cell migration, proliferation and death.

Standard models of biological and ecological systems are based on the mean field assumption which, roughly speaking, assumes that individuals in the population encounter each other in proportion to their average density (Law and Dieckmann, 2000). Classical examples of mean field models include Lotka-Volterra models of ecological competition (Murray 1989), the Keller-Segel model of chemotaxis (Keller and Segel 1971), the logistic growth model (Edelstein-Keshet 2005), and many others including models of gene expression (Shreshtha et al. 2016). Standard models based on ordinary and partial differential equations typically invoke the mean field assumption, either explicitly or implicitly. In this work we take a more general approach by accounting for spatial correlations present in the population. In particular we study the population dynamics in terms of the dynamics of spatial moments, which accounts for the dynamics of individuals, dynamics of pairs of individuals, and so on (Plank and Law, 2015). This approach means that we do not need to rely on performing a large number of repeated stochastic simulations to understand the population dynamics. This benefit comes with the added complication that we have to deal with an infinite system of equations governing the spatial moments of the system. To deal with this, we use a moment closure approximation to give a tractable finite system of moment equations (Murrell et al. 2004; Raghib et al. 2011).

The first studies that used spatial moments focused on modelling birth-death processes in ecology with a single species (Bolker and Pacala 1997; Lewis 2000), and later studies examined competition and prey-predator interactions in a multi-species birth-death framework (Murrell 2005; Barraquand and Murrell 2013). More recently these kinds of ecological models have been extended to include birth, death and movement processes that are motivated by observations from cell biology experiments (Baker and Simpson 2010; Simpson et al. 2013). However, these first models that include cell migration are lattice-based, which means that the movement of individuals is restricted to an artificial lattice (Plank and Simpson 2012). Lattice-free moment dynamics models of cell migration and cell proliferation have also been presented (Middleton et al. 2014; Binny et al. 2015, 2016a, 2016b). Unlike the lattice-based models in which volume exclusion effects are strictly enforced (Dyson and Baker 2015; Bruna and Chapman 2012), lattice-free models use interaction kernels to describe interactions and crowding effects. This approach is more biologically realistic than hard sphere interactions as cells are able to deform as they move close to neighboring cells (Le Clainche and Carlier 2008). In this work we present a lattice-free model of cell migration, cell proliferation and cell death. In an attempt to make the model relevant to *in vivo* conditions, we take a multi-species approach where we consider one species to be a population of motile and proliferative cells, whereas the other population represents an immobile subpopulation of obstacles.

bioRxiv preprint doi: https://doi.org/10.1101/267708; this version posted February 18, 2018. The copyright holder for this preprint (which was not certified by peer review) is the author/funder. All rights reserved. No reuse allowed without permission.



This manuscript is organised in the following way. In Section 2, we describe the IBM, and explain the different features of the model, the notation and the simulation method. In Section 3, we give a comprehensive description of crowding effects and the nature of neighbor-dependent directional bias in terms of the bias landscape which explicitly accounts for cell-to-cell interactions, and cell-to-obstacle interactions. In Section 4, we derive a moment dynamics description of the IBM to provide a means of analysing the model. In Section 5, we present stochastic simulation results to explore how the presence and characteristics of obstacles influence the dynamics of the population of cells. Finally, in section 6, we summarise our findings and conclusions.

## 2 Individual-based model

We consider an IBM to describe the movement, proliferation and death of individuals within a population composed of many subpopulations. One possible application of the IBM would be to describe the collective dynamics of a population of motile biological cells, where individual cells in the population undergo movement, proliferation and death events. An important feature of our model is that we explicitly incorporate crowding effects. For example, these effects are able to accommodate contact inhibition of proliferation and/or contact inhibition of migration, where the ability of individuals to either proliferate or migrate is reduced in regions of high density (Warne et al. 2017; Vedel et al. 2013). Another key feature of the IBM is that it permits the simulation of different types of subpopulations within the total population. This gives great flexibility since the model can be used to study the movement, proliferation and death of different types of individuals, and it also allows for different types of interactions between the different subpopulations. The state of the IBM depends on the position of each individual, and the properties of agents within each subpopulation. In the model, we have a total of $N(t)$ agents that are associated with $I$ subpopulations. The location of the $n^{\text{th}}$ agent is $\mathbf{x}_n \in \mathbb{R}^2$, and each agent belongs to a particular subpopulation, $i_n \in \{1, 2, \ldots, I\}$, where $n = 1, 2, \ldots, N(t)$. We always initiate the IBM with a random spatial distribution of individuals. This means that our model is relevant for spatially homogeneous problems without macroscopic gradients in density of individuals.

Individuals undergo movement, proliferation and death events with a rate per unit time given by $\widehat{M}_n, \widehat{P}_n$ and $\widehat{D}_n$ respectively. The IBM is a continuous-time Markov process, where the probability of agent $n$ undergoing a movement during a short time interval, of duration $\delta t$, is $\widehat{M}_n \delta t + O(\delta t^2)$. Similar expressions govern the probability of proliferation and death events occurring within a short time interval. The total event rates are comprised of a neighbor independent, intrinsic component, and a neighbor-dependent component accounting for interactions with neighboring individuals. The neighborhood contribution is specified by an interaction kernel that depends upon the displacement, $\boldsymbol{\xi}$ between pairs of individuals. We assume the interaction kernel

bioRxiv preprint doi: https://doi.org/10.1101/267708; this version posted February 18, 2018. The copyright holder for this preprint (which was not certified by peer review) is the author/funder. All rights reserved. No reuse allowed without permission.



is isotropic and decays to zero at larger distances, $|\boldsymbol{\xi}|$, ensuring that only relatively close individuals have a significant interaction. For movement events, the intrinsic component of the movement rate of an individual of type $i$ is denoted by $m_i$, and the neighbor dependency from a neighboring individual of type $j$ is governed by an interaction kernel $\omega_{ij}^{(m)}(\boldsymbol{\xi})$. Hence we write the net movement rate of individual $n$ of type $i$ as,

$$\widehat{M}_n = \max\left(0, m_{i_n} + \sum_{r\neq n} \omega_{i_n j_r}^{(m)}(\mathbf{x}_r - \mathbf{x}_n)\right). \tag{1}$$

Similarly, we write the net proliferation and net death rates as,

$$\widehat{P}_n = \max\left(0, p_{i_n} + \sum_{r\neq n} \omega_{i_n j_r}^{(p)}(\mathbf{x}_r - \mathbf{x}_n)\right), \tag{2}$$

$$\widehat{D}_n = \max\left(0, d_{i_n} + \sum_{r\neq n} \omega_{i_n j_r}^{(d)}(\mathbf{x}_r - \mathbf{x}_n)\right), \tag{3}$$

where $p_i$ and $d_i$ are the intrinsic proliferation and death rates, respectively, for an agent of type $i$. This description of the IBM is equivalent to the spatially homogeneous model presented by Plank and Law (2015). For simplicity, we assume a constant death rate and a fixed distribution for the direction of placement of daughter agents which is not affected by the interactions with other individuals when we implement the IBM.

When an individual of type $i$ undergoes a movement event, it travels a displacement $\boldsymbol{\xi}$ that is drawn from a probability density function (PDF) $\mu_i^{(m)}(\boldsymbol{\xi})$. If an individual of type $i$ proliferates, a daughter of the same type is placed at a displacement $\boldsymbol{\xi}$, that is drawn from a PDF $\mu_i^{(p)}(\boldsymbol{\xi})$. Now we generalise the movement PDF by introducing a neighbor-dependent bias vector, to accommodate the influence of neighboring individuals upon the direction of movement. We introduce an interaction kernel, $\omega_{ij}^{(b)}(\boldsymbol{\xi})$, to account for neighbor-dependent directional bias acting on the reference individual, of type $i$, due to the presence of a second individual, of type $j$, at a displacement $\boldsymbol{\xi}$. The neighbor-dependent bias is defined as the gradient of interaction kernel, $\nabla\omega_{ij}^{(b)}(\boldsymbol{\xi})$. This definition is same as that of Binny et al. (2016b), however here we generalize that previous model to account for the contributions to the directional bias arising from multiple species present within the total population. The net bias vector is the sum of contributions from each of the neighboring individuals, and a constant neighbor-independent global bias $\mathbf{b}_{i_n} \in \mathbb{R}^2$, giving

$$\widehat{\mathbf{B}}_n = \mathbf{b}_{i_n} + \sum_{r\neq n} \nabla\omega_{i_n j_r}^{(b)}(\mathbf{x}_r - \mathbf{x}_n). \tag{4}$$

The angular direction of the net bias vector, denoted by $\arg(\widehat{\mathbf{B}}_n) \in [0, 2\pi]$, is the preferred direction of movement for a particular individual. In this framework, the preferred direction of movement is driven, in part, by the sum of the

bioRxiv preprint doi: https://doi.org/10.1101/267708; this version posted February 18, 2018. The copyright holder for this preprint (which was not certified by peer review) is the author/funder. All rights reserved. No reuse allowed without permission.



gradient of the interaction kernels. The strength of bias is given by the magnitude of bias vector, $|\widehat{\mathbf{B}}_n|$. Now we assume that the neighboring individuals affect the direction of movement $\arg(\boldsymbol{\xi}) \in [0, 2\pi]$, but not the actual distance moved, $|\boldsymbol{\xi}|$.

During a movement event, the direction of movement is drawn from a von Mises distribution, $\mathrm{g}(\theta; \widehat{\mathbf{B}}_n)$ whose concentration parameter is $|\widehat{\mathbf{B}}_n|$, and the mean direction is given by $\arg(\widehat{\mathbf{B}}_n)$,

$$\mathrm{g}(\theta; \widehat{\mathbf{B}}_n) = \frac{\exp\Big(|\widehat{\mathbf{B}}_n| \cos\Big(\theta - \arg(\widehat{\mathbf{B}}_n)\Big)\Big)}{2\pi \mathrm{I}_0\big(|\widehat{\mathbf{B}}_n|\big)}, \tag{5}$$

where $I_0$ is the zeroth order modified Bessel function (Abramowitz and Stegun 1972). This PDF ensures that individuals are most likely move in the direction of $\arg(\widehat{\mathbf{B}}_n)$, and the bias to move in this preferred direction increases with $|\widehat{\mathbf{B}}_n|$. When the net bias is zero, $\widehat{\mathbf{B}}_n = \mathbf{0}$, the von Mises distribution reduces to the uniform distribution (Binny et al. 2016b). Individuals located where the gradient is steep will have a large $|\widehat{\mathbf{B}}_n|$, hence they are more likely to move in the direction of $\widehat{\mathbf{B}}_n$. On the other hand, individuals located where the gradient is relatively flat will have a weaker bias. As a result, the direction of movement of those individuals becomes almost uniformly distributed (Browning et al. 2017). We assume that the distance moved by an agent is independent of local crowding, and is given by a fixed PDF, $u_i(|\boldsymbol{\xi}|)$. Hence the net movement PDF is the product of the distance PDF and the direction PDF, giving

$$\mu_i^{(m)}(\boldsymbol{\xi}; \widehat{\mathbf{B}}_n) = u_i(|\boldsymbol{\xi}|)\mathrm{g}(\arg(\boldsymbol{\xi}); \widehat{\mathbf{B}}_n). \tag{6}$$

### 2.1 Description of IBM for a population of motile, proliferative agents in an environment containing obstacles

The IBM can be applied to numerous problems involving populations composed of various combinations of motile and stationary subpopulations by appropriate choice of parameters. Here we focus on one specific scenario with two distinct subpopulations, $I = 2$. We consider the first subpopulation to be a group of agents undergoing movement, proliferation and death events. This first subpopulation can be thought of as a population of motile, proliferative cells. The first subpopulation interacts with a second subpopulation that is composed of stationary, non-proliferating obstacles. The event rates for individual agents in the first subpopulation will be influenced by the presence of both obstacles and other agents in their neighborhood, given by Equations (1)-(3). Since the obstacles never undergo birth, death or movement events, they contribute to the overall dynamics by interactions between the obstacles and the agents.

We introduce interaction kernels: $\omega_{ij}^{(m)}(\boldsymbol{\xi})$; $\omega_{ij}^{(p)}(\boldsymbol{\xi})$; and $\omega_{ij}^{(b)}(\boldsymbol{\xi})$, to account for the contribution from surrounding agents and obstacles to the movement

bioRxiv preprint doi: https://doi.org/10.1101/267708; this version posted February 18, 2018. The copyright holder for this preprint (which was not certified by peer review) is the author/funder. All rights reserved. No reuse allowed without permission.



rate, proliferation rate, and the directional bias of an agent, respectively. We choose these interaction kernels to be two-dimensional Gaussian functions. The movement interaction kernel is given by,

$$\omega_{ij}^{(m)}(\boldsymbol{\xi}) = \gamma_{ij}^{(m)} \exp\left(-\frac{|\boldsymbol{\xi}|^2}{2(\sigma_{ij}^{(m)})^2}\right), \tag{7}$$

where $\gamma_{ij}^{(m)}$ and $\sigma_{ij}^{(m)} > 0$ represent the interaction strength and the spatial extent of interaction, respectively. We assume a similar form for the proliferation and bias kernels, given by,

$$\omega_{ij}^{(p)}(\boldsymbol{\xi}) = \gamma_{ij}^{(p)} \exp\left(-\frac{|\boldsymbol{\xi}|^2}{2(\sigma_{ij}^{(p)})^2}\right), \tag{8}$$

$$\omega_{ij}^{(b)}(\boldsymbol{\xi}) = \gamma_{ij}^{(b)} \exp\left(-\frac{|\boldsymbol{\xi}|^2}{2(\sigma_{ij}^{(b)})^2}\right). \tag{9}$$

In our simulations we have two subpopulations. The first subpopulation, denoted $i = 1$, corresponds to the motile and proliferative agents. The second subpopulation, denoted $i = 2$, corresponds to the stationary, non-proliferative obstacles. The intrinsic rates of movement and proliferation of agents are $m_1$ and $p_1$, respectively. These rates for obstacles are zero. The presence of subpopulations of agents and obstacles results in different types of interactions. The interactions involving the pairs of individuals of same type such as, agent-agent and obstacle-obstacle pairs, are specified by $\omega_{11}^{(m)}(\boldsymbol{\xi})$ and $\omega_{22}^{(m)}(\boldsymbol{\xi})$, respectively. Similar kernels apply for proliferation and bias. Interactions involving individuals from different subpopulations are specified by the interaction kernels $\omega_{12}^{(m)}(\boldsymbol{\xi})$ and $\omega_{21}^{(m)}(\boldsymbol{\xi})$. Since obstacles are both stationary and non-proliferative, the presence of neighboring agents and obstacle does not affect the dynamics and spatial arrangement of obstacles in any way. Hence the interaction strengths $\gamma_{21}^{(m)}$ and $\gamma_{22}^{(m)}$ are both set to zero. Positive $\gamma_{11}^{(m)}$ and $\gamma_{12}^{(m)}$ values enhance the movement rate of agents, and can be thought of as representing contact stimulation of migration. In contrast, a negative interaction strength results in a reduction of the movement rate, which can be thought of as representing contact inhibition of migration. Similarly, the net proliferation rate of agents, and the nature of directional bias depend on the sign of interaction strength.

We use a univariate Gaussian distribution, with mean $\mu_1^{(s)}$ and standard deviation $\sigma_1^{(s)}$, to specify the distribution of movement distance for agents $u_1(\boldsymbol{\xi})$. The movement displacement kernels, $\mu_{11}^{(m)}(\boldsymbol{\xi}, t)$ and $\mu_{12}^{(m)}(\boldsymbol{\xi}, t)$, also require the specification of the movement distance distribution, $u_1(\boldsymbol{\xi})$, and the neighbor-dependent direction probability density function given by Equation

bioRxiv preprint doi: https://doi.org/10.1101/267708; this version posted February 18, 2018. The copyright holder for this preprint (which was not certified by peer review) is the author/funder. All rights reserved. No reuse allowed without permission.



(5). For simplicity, the dispersal kernel $\mu_1^{(p)}(\boldsymbol{\xi})$ is chosen to be neighbor independent, and specified as a bivariate Gaussian distribution with zero mean and standard deviation $\sigma_1^{(d)}$.

## 2.2 Numerical implementation

We simulate the IBM using the Gillespie algorithm (Gillespie 1977). In each simulation the population is initially composed of $N_1(0)$ agents and $N_2(0)$ obstacles, distributed according to a spatial Poisson process across a square domain of size $L \times L$. This configuration ensures the absence of spatial structure in the initial population. The movement, proliferation and death rates of the agents are computed using Equations (1)-(3). For this study, we use a constant death rate for all the agents, hence the neighbor-dependent term in Equation (3) is set to zero. The sum of event rates of all agents is given by,

$$\lambda(t) = \sum_{n=1}^{N_1(t)} \left(\widehat{M}_n + \widehat{P}_n + \widehat{D}_n\right). \tag{10}$$

Since the event rates for obstacles are always zero, those terms do not contribute to $\lambda(t)$. The time interval between consecutive events is exponentially distributed with mean $1/\lambda(t)$. At each event time, one of the three possible events occurs to an agent. The probability of occurrence of an event is proportional to the rate of that event. For a movement event, the agent moves a displacement specified by the bias vector and movement kernel in Equation (4) and Equation (6), respectively. For a proliferation event, the proliferative agent places a daughter agent at a displacement specified by dispersion kernel $\mu_1^{(p)}(\boldsymbol{\xi})$, and the total number of agents increases by one. For a death event the total number of agents is reduced by one.

To provide a mathematical description of the IBM we analyse the dynamics of the first and second spatial moments of the agents and obstacles. The first moment of agents and obstacles is given by dividing the total number of agents and obstacles by the area of the domain, giving $N_1(t)/L^2$ and $N_2(t)/L^2$, respectively. We use a pair correlation function (PCF) to quantify the second spatial moment. Here the PCF depends on both the separation distance, $r$, and time, $t$. However, to be consistent with previous studies, our notation will explicitly focus on the separation distance, $r$. Since there are two different subpopulations, we will have two different PCFs. First, we denote the auto-correlation PCF between agents as $C_{11}(r)$. Second, we denote the cross-correlation between agents and obstacles as $C_{12}(r)$. To compute the auto-correlation function, we consider a reference agent at $\mathbf{x}_i$, and calculate all distances, $r = |\mathbf{x}_j - \mathbf{x}_i|$, to the other $N_1 - 1$ agents. We follow the same procedure with each of the remaining agents until all agents have acted as the reference agent. Note that we always take care to measure distances across periodic boundaries. With this information, the auto-correlation PCF is constructed by enumerating the distances between pairs of agents that fall into the

bioRxiv preprint doi: https://doi.org/10.1101/267708; this version posted February 18, 2018. The copyright holder for this preprint (which was not certified by peer review) is the author/funder. All rights reserved. No reuse allowed without permission.



interval, $\left[r-\delta r/2, r+\delta r/2\right]$. That means we use a bin width of $\delta r$. To ensure that $C_{11}(r)=1$ in the absence of spatial structure, we normalize the bin count by a factor of $N_1(t)(N_1(t)-1)(2\pi r\delta r)/L^2$. When $C_{11}(r)>1$, we have a larger number of pairs of agents separated by a distance $r$ than we would have in the spatially random population. In contrast, for $C_{11}(r)<1$, we have a smaller number of pairs of agents separated by a distance $r$ than we would have in the spatially random population. Similarly, we compute the cross-correlation PCF, $C_{12}(r)$, by counting, binning and normalizing all distances between agents and obstacles. A similar calculation could be made for $C_{22}(r)$, by counting, binning and normalizing all distances between pairs of obstacles. However, since obstacles are stationary, non-proliferative and initialized at random, we always have $C_{22}(r)=1$. Only when $C_{11}(r)=C_{12}(r)=C_{22}=1$ are agents and obstacles are arranged at random, which is an implicit assumption in all mean-field models. One of the important features of our model and our analysis is that we can have spatial structure, such as clustering and segregation, present in the population. This is signified by having $C_{11}(r)\neq 1$ and $C_{12}(r)\neq 1$.

There are several key variables relevant to specifying different obstacle fields and different obstacle properties. These include obstacle density, obstacle size and obstacle interactions, such as whether obstacles are adhesive or repulsive. We will now explore how systematically varying these properties influences the development of spatial structure in a population of motile and proliferative agents that are placed into an environment containing obstacles. We first explore this by performing repeated realisations of the IBM and analysing averaged ensemble data in terms of the first spatial moment and PCF. Second, we then compare these results with the prediction from our analysis of spatial moment dynamics in Section 5. A summary of key variables and notation for these calculations is given in Table 1.

## 3 Bias landscape

One key feature of the IBM is the neighbor-dependent bias. This formalism helps us in understanding how the spatial arrangement of obstacles and other agents affects the movement of a particular reference agent. To interpret and visualize the neighbor-dependent bias, we define the *bias landscape* as,

$$C(\mathbf{x}) = C_1(\mathbf{x}) + C_2(\mathbf{x}), \tag{11}$$

where,

$$C_1(\mathbf{x}) = \sum_{n\in N_1} \omega_{11}^{(b)}(\mathbf{x}_n - \mathbf{x}), \tag{12}$$

$$C_2(\mathbf{x}) = \sum_{n\in N_2} \omega_{12}^{(b)}(\mathbf{x}_n - \mathbf{x}), \tag{13}$$

are contributions to overall bias landscape from the agents and the obstacles, respectively. For an agent located at $\mathbf{x}$, $C(\mathbf{x})$ acts as a measure of the degree

bioRxiv preprint doi: https://doi.org/10.1101/267708; this version posted February 18, 2018. The copyright holder for this preprint (which was not certified by peer review) is the author/funder. All rights reserved. No reuse allowed without permission.



**Table 1** Model parameters and typical values.

| Parameter | Symbol | Value |
|---|---|---|
| **Densities** | | |
| Agents | $Z_{1,1}(t)$ | 0.25 to 0.9 |
| Obstacles | $Z_{1,2}(t)$ | 0.0 to 0.375 |
| Initial density of agents | $Z_{1,1}(0)$ | 0.25 |
| Initial density of obstacles | $Z_{1,2}(0)$ | 0.0 to 0.375 |
| **Intrinsic rates** | | |
| Birth | $p_1$, $p_2$ | 1, 0 |
| Death | $d_1$, $d_2$ | 0.5, 0 |
| Movement | $m_1$, $m_2$ | 5, 0 |
| **Neighbor-dependent interaction strengths** | | |
| Birth | $\gamma_{11}^{(p)}$, $\gamma_{12}^{(p)}$, $\gamma_{21}^{(p)}$, $\gamma_{22}^{(p)}$ | -0.38 to 0 |
| Movement | $\gamma_{11}^{(m)}$, $\gamma_{12}^{(m)}$, $\gamma_{21}^{(m)}$, $\gamma_{22}^{(m)}$ | 0 |
| Bias | $\gamma_{11}^{(b)}$, $\gamma_{12}^{(b)}$, $\gamma_{21}^{(b)}$, $\gamma_{22}^{(b)}$ | -0.2 to 0.4 |
| **Spatial extent of interactions** | | |
| Birth | $\sigma_{11}^{(p)}$, $\sigma_{12}^{(p)}$, $\sigma_{21}^{(p)}$, $\sigma_{22}^{(p)}$ | 0.25 to 0.6 |
| Movement | $\sigma_{11}^{(m)}$, $\sigma_{12}^{(m)}$, $\sigma_{21}^{(m)}$, $\sigma_{22}^{(m)}$ | 0.25 to 0.6 |
| Bias | $\sigma_{11}^{(b)}$, $\sigma_{12}^{(b)}$, $\sigma_{21}^{(b)}$, $\sigma_{22}^{(b)}$ | 0.25 to 0.6 |
| **Movement and dispersion distance** | | |
| Mean movement distance | $\mu_1^{(s)}$, $\mu_2^{(s)}$ | 0.4 |
| Standard deviation movement distance | $\sigma_1^{(s)}$, $\sigma_2^{(s)}$ | 0.1 |
| Standard deviation dispersion distance | $\sigma_1^{(d)}$, $\sigma_2^{(d)}$ | 0.5 |

of crowding. The neighbor-dependent bias vector, $\mathbf{B}_n$, is the negative gradient of the bias landscape, $-\nabla C(\mathbf{x})$. With these definitions it is straightforward to see that agents in the model move in response to the gradient of the bias landscape. Writing the negative gradient of the bias landscape in terms of the contributions from the two subpopulations, $-\nabla C(\mathbf{x}) = -\nabla C_1(\mathbf{x}) - \nabla C_2(\mathbf{x})$, it is clear that the spatial arrangements of both the agents and the obstacles play a role in influencing the movement of agents in the IBM.

The influence of bias depends on the spatial arrangement of the agents and obstacles, and properties of the interaction kernels, $\omega_{11}^{(b)}(\boldsymbol{\xi})$ and $\omega_{12}^{(b)}(\boldsymbol{\xi})$, respectively. When the kernels are decreasing functions of $\boldsymbol{\xi}$, agents experience a repulsive bias that encourages them to move away from the regions of high crowding. Figure 1 shows how the repulsive bias affects the movement of agents in a particular arrangement of agents and stationary obstacles. The bias landscape and corresponding level curves due to agent-agent interactions alone are shown in Figure 1(a)-(b). The locations of agents are represented by red dots, and the arrows indicate the preferred direction of movement. The length of these arrows indicates the strength of bias. We note that crowded agents experience a strong repulsive bias, and prefer to move towards a lower density region. Figure 1(c)-(d) shows the crowding effects generated by obstacles only, and Figure 1(e)-(f) shows how both the agent-agent and agent-obstacle

bioRxiv preprint doi: https://doi.org/10.1101/267708; this version posted February 18, 2018. The copyright holder for this preprint (which was not certified by peer review) is the author/funder. All rights reserved. No reuse allowed without permission.



interactions sum to give the total bias landscape. Note that, if the bias interaction strength is negative, then the interaction kernels $\omega_{11}^{(b)}(\boldsymbol{\xi})$ and $\omega_{12}^{(b)}(\boldsymbol{\xi})$ are increasing functions of $\boldsymbol{\xi}$. In that case, the orientation of the bias landscape structure would be reversed, and we would have an attractive bias.

bioRxiv preprint doi: https://doi.org/10.1101/267708; this version posted February 18, 2018. The copyright holder for this preprint (which was not certified by peer review) is the author/funder. All rights reserved. No reuse allowed without permission.



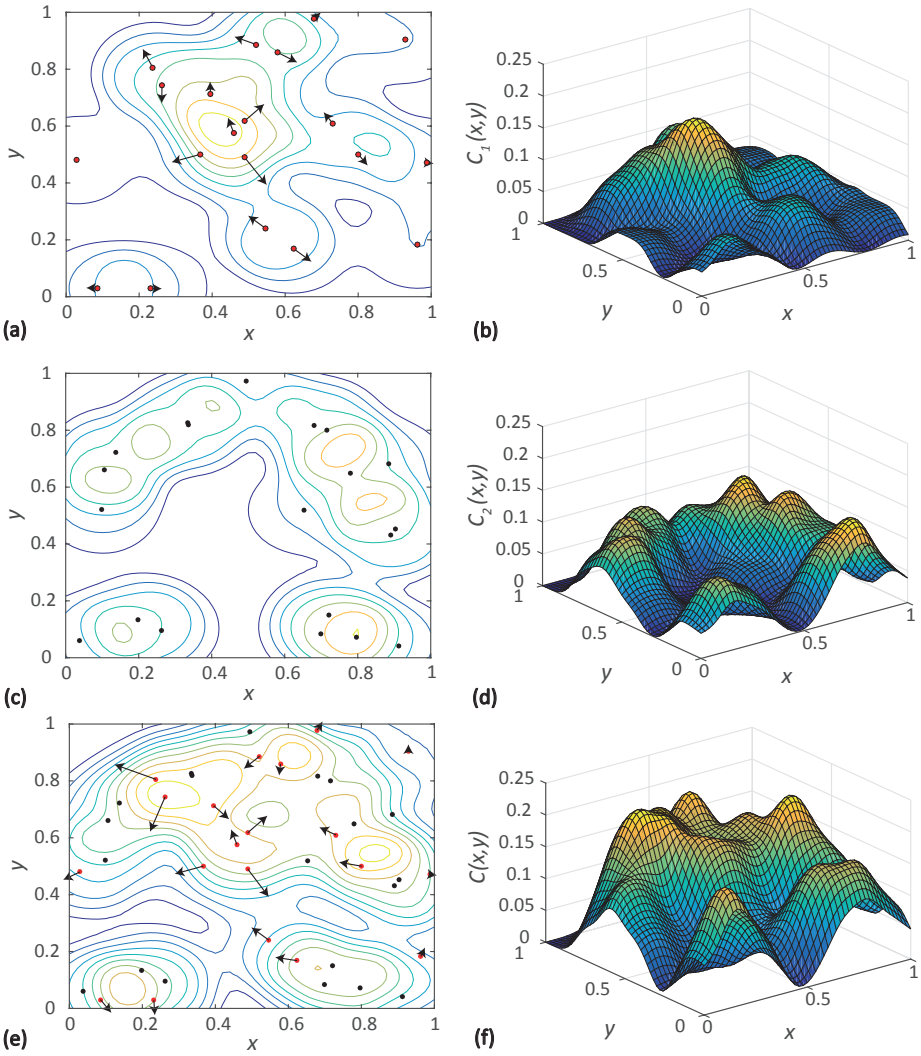


**Fig. 1** Effect of neighbor dependent bias visualized for a particular arrangement of 20 agents (red dots) and 20 obstacles (black dots). In this case we have a positive Gaussian interaction kernel to specify the interactions among agents as well as the interactions between agents and obstacles. **a** Shows the locations of agents (red dots). **b** Shows the location of obstacles (black dots). **c** Shows the location of both agents (red dots) and obstacles (black dots). In each subfigure, **a,c,e**, the locations of individuals are superimposed with the level curves of various components of the bias landscape. **b,d,f** shows the different components of the bias landscape: $C_1(\mathbf{x})$; $C_2(\mathbf{x})$; and $C(\mathbf{x})$, respectively. The bias vectors in **a** show $-\nabla C_1(\mathbf{x}_n)$, which is the negative gradient of the component of the bias landscape corresponding to agent-agent interactions. The bias vectors in **c** show $-\nabla C(\mathbf{x}_n)$, which is the negative gradient of the net bias landscape corresponding to the sum of agent-agent and agent-obstacle interactions. The length of arrows indicate the strength of bias. Results in **a-b** correspond to interactions between agents only. Results in **c-d** show interactions between obstacles. Results in **e-f** show the net interactions between agents and obstacles. Parameters are $\gamma_{11}^{(b)} = \gamma_{12}^{(b)} = 0.2$ and $\sigma_{11}^{(b)} = \sigma_{12}^{(b)} = 0.5$
.

bioRxiv preprint doi: https://doi.org/10.1101/267708; this version posted February 18, 2018. The copyright holder for this preprint (which was not certified by peer review) is the author/funder. All rights reserved. No reuse allowed without permission.



Another key variable in the IBM is the size of the obstacles, which determines the spatial extent of the obstacle-agent bias. We use the parameter describing the spatial extent of interactions, $\sigma_{12}^{(b)}$, as a proxy for obstacle size. Here we make the natural assumption that larger obstacles correspond to increased $\sigma_{12}^{(b)}$, so that larger obstacles tend to exert an influence over a larger neighborhood. Note that we maintain the bias strength, $\gamma_{12}^{(b)}$, as a constant and we only vary $\sigma_{12}^{(b)}$ to mimic the influence of obstacle size. Results in Figure 2 show the same spatial arrangement of 20 agents and 20 obstacles as in Figure 1, except that we reduce $\sigma_{12}^{(b)}$ so that the obstacles in Figure 2 influence a smaller neighborhood than the obstacles in Figure 1. This change in obstacle size does not affect the agent-agent component of the bias landscape, $C_1(\mathbf{x})$, but it does affect the agent-obstacle component, $C_2(\mathbf{x})$.

bioRxiv preprint doi: https://doi.org/10.1101/267708; this version posted February 18, 2018. The copyright holder for this preprint (which was not certified by peer review) is the author/funder. All rights reserved. No reuse allowed without permission.



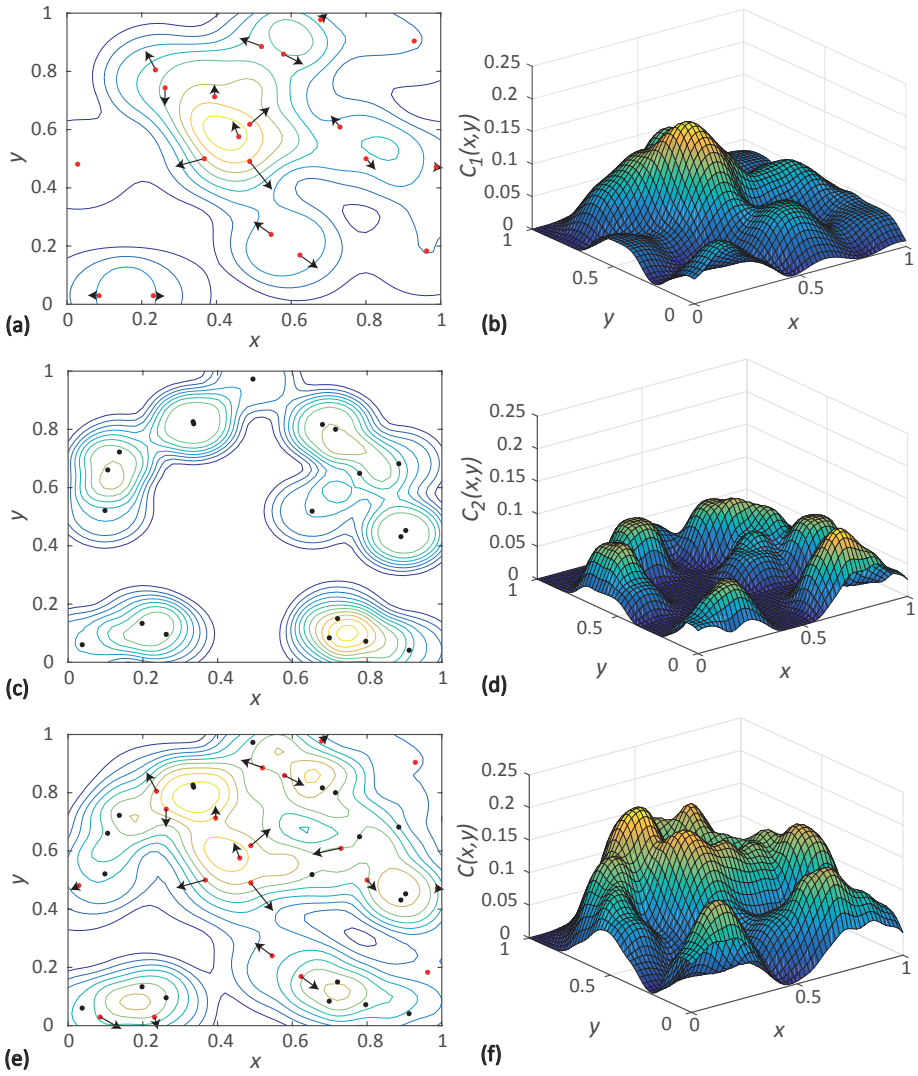


**Fig. 2** Effect of neighbor dependent bias visualized for a particular arrangement of 20 agents (red dots) and 20 smaller obstacles (black dots). In this case we have a positive Gaussian interaction kernel to specify the interactions among agents as well as the interactions between agents and obstacles. **a** Shows the locations of agents (red dots). **b** Shows the location of obstacles (black dots). **c** Shows the location of both agents (red dots) and obstacles (black dots). In each subfigure, **a,c,e**, the locations of individuals are superimposed with the level curves of various components of the bias landscape. **b,d,f** shows the different components of the bias landscape: $C_1(\mathbf{x})$; $C_2(\mathbf{x})$; and $C(\mathbf{x})$, respectively. The bias vectors in **a** show $-\nabla C_1(\mathbf{x}_n)$, which is the negative gradient of the component of the bias landscape corresponding to agent-agent interactions. The bias vectors in **c** show $-\nabla C(\mathbf{x}_n)$, which is the negative gradient of the net bias landscape corresponding to the sum of agent-agent and agent-obstacle interactions. The length of arrows indicate the strength of bias. Results in **a-b** correspond to interactions between agents only. Results in **c-d** show interactions between obstacles. Results in **e-f** show the net interactions between agents and obstacles. Parameters are $\gamma_{11}^{(b)} = \gamma_{12}^{(b)} = 0.2$, $\sigma_{11}^{(b)} = 0.5$ and $\sigma_{12}^{(b)} = 0.25$

.

bioRxiv preprint doi: https://doi.org/10.1101/267708; this version posted February 18, 2018. The copyright holder for this preprint (which was not certified by peer review) is the author/funder. All rights reserved. No reuse allowed without permission.



## 4 Spatial moment dynamics

Here, we derive a continuum approximation for the IBM in terms of spatial moments. We present the derivation for a general case where we consider an arbitrary number of motile and proliferative subpopulations. Then we present a specific model that can be used to describe a special case where there are two subpopulations: the first subpopulation is a population of motile and proliferative agents that can be thought of as biological cells, and the second subpopulation is a population of stationary and non-proliferative obstacles.

### 4.1 Definition of spatial moments for general multi-species model

Let us define a random variable, $N_i(A)$, to be the number of agents of type $i$ in a region $A \subset R^2$ at a given time $t$. Let $D_h(\mathbf{x}) \subset R^2$ denote a disc of radius $h$ centered on $\mathbf{x} \in R^2$. As mentioned in the Introduction, we consider a spatially homogeneous environment, which means the probability of finding an agent in a given small region is independent of the position of that small region in space. Hence the key quantity of interest is the distance between agents (Binny et al. 2016a; Baker and Simpson, 2010). Since we are considering population dynamics in a spatially homogeneous environment, we assume without loss of generality that one of the agents is located at the origin, $\mathbf{x} = \mathbf{0}$.

In our simulations, we approximate the first spatial moment, $Z_{1,i}(t)$, by dividing the population size of agents of type $i$, given by $N_i(t)$, by the area of the domain, $L^2$. Formally we have,

$$Z_{1,i}(t) = \lim_{h\to 0} \frac{1}{h} \mathbb{E}\Big[N_i\big(D_h(\mathbf{0})\big)\Big]. \tag{14}$$

The second spatial moment, $Z_{2,ij}(\boldsymbol{\xi}, t)$, is the average density of pairs of agents. For a pair of individuals consisting of an agent of type $i$ present at $\mathbf{x} = \mathbf{0}$, and an agent of type $j$ present at a displacement $\boldsymbol{\xi}$, we have

$$Z_{2,ij}(\boldsymbol{\xi}, t) = \lim_{h\to 0} \frac{1}{h^2} \mathbb{E}\Big[N_i(D_h(\mathbf{0}))N_j(D_h(\boldsymbol{\xi})) - \delta_{ij} N_i(D_h(\mathbf{0}) \cap D_h(\boldsymbol{\xi}))\Big]. \tag{15}$$

The second term in the expectation in Equation (15) is necessary to avoid counting self-pairs. If the discs $D_h(\mathbf{0})$ and $D_h(\boldsymbol{\xi})$ are non-overlapping, this term becomes zero (Plank and Law 2015). The third spatial moment is the density of triplets of agents, and is similarly defined as,

$$\begin{aligned} Z_{3,ijk}(\boldsymbol{\xi}, \boldsymbol{\xi'}, t) = \lim_{h\to 0} \frac{1}{h^3} \mathbb{E}\Big[ & N_i(D_h(\mathbf{0}))N_j(D_h(\boldsymbol{\xi}))N_k(D_h(\boldsymbol{\xi'})) \\ & - \delta_{ij} N_i(D_h(\mathbf{0}) \cap D_h(\boldsymbol{\xi}))N_k(D_h(\boldsymbol{\xi'})) \\ & - \delta_{ik} N_i(D_h(\mathbf{0}) \cap D_h(\boldsymbol{\xi'}))N_j(D_h(\boldsymbol{\xi})) \\ & - \delta_{jk} N_j(D_h(\boldsymbol{\xi}) \cap D_h(\boldsymbol{\xi'}))N_i(D_h(\mathbf{0})) \\ & + 2\delta_{ijk} N_i(D_h(\mathbf{0}) \cap D_h(\boldsymbol{\xi'}) \cap D_h(\boldsymbol{\xi}))\Big]. \end{aligned} \tag{16}$$

bioRxiv preprint doi: https://doi.org/10.1101/267708; this version posted February 18, 2018. The copyright holder for this preprint (which was not certified by peer review) is the author/funder. All rights reserved. No reuse allowed without permission.



Again, the extra terms in Equation (16) are needed to avoid counting non-distinct triplets.

### 4.2 Dynamics of spatial moments

The expected rates of movement and proliferation of an agent, denoted by $M_{1,i}(t)$ and $P_{1,i}(t)$, depend on the contribution from another agent at a displacement $\boldsymbol{\xi}$. The conditional probability of having an agent of type $j$ at a displacement $\boldsymbol{\xi}$ given that an agent of type $i$ is located at $\mathbf{0}$, is given by $Z_{2,ij}(\boldsymbol{\xi},t)/Z_{1,i}(t)$. The expected movement and proliferation rates of an agent of type $i$ is given by multiplying this conditional probability by the corresponding interaction kernels, $\omega_{ij}^{(m)}(\boldsymbol{\xi})$ or $\omega_{ij}^{(p)}(\boldsymbol{\xi})$, respectively, and integrating over all possible displacements, giving

$$M_{1,i}(t) = m_i + \sum_j \int \omega_{ij}^{(m)}(\boldsymbol{\xi}) \frac{Z_{2,ij}(\boldsymbol{\xi},t)}{Z_{1,i}(t)} \,\mathrm{d}\boldsymbol{\xi}, \tag{17}$$

$$P_{1,i}(t) = p_i + \sum_j \int \omega_{ij}^{(p)}(\boldsymbol{\xi}) \frac{Z_{2,ij}(\boldsymbol{\xi},t)}{Z_{1,i}(t)} \,\mathrm{d}\boldsymbol{\xi}. \tag{18}$$

We now consider the dynamics of the first moment. The first moment dynamics depends solely upon the balance between the expected rate of proliferation, $P_{1,i}(t)$, and death rate, $d_i$. The movement and neighbor-dependent directional bias does not directly influence the dynamics of the first moment. The time evolution of the first moment is given by,

$$\frac{\mathrm{d}}{\mathrm{d}t} Z_{1,i}(t) = \Big(P_{1,i}(t) - d_i\Big) Z_{1,i}(t). \tag{19}$$

The dynamics of average density of pairs of agents depends on the conditional occupancy of a third agent in the neighborhood. The conditional probability of having an agent of type $k$ located at a displacement $\boldsymbol{\xi'}$, given that a pair of agents consisting of type $j$ and $i$, where each of them are located at $\boldsymbol{\xi}$ and $\mathbf{0}$, respectively, is $Z_{3,ijk}(\boldsymbol{\xi},\boldsymbol{\xi'},t)/Z_{2,ij}(\boldsymbol{\xi},t)$. Hence the expected rate of movement and proliferation is found by multiplying $Z_{3,ijk}(\boldsymbol{\xi},\boldsymbol{\xi'},t)/Z_{2,ij}(\boldsymbol{\xi},t)$ by the interaction kernels and integrating over all possible displacements as follows,

$$M_{2,ij}(\boldsymbol{\xi},t) = m_i + \sum_k \int \omega_{ik}^{(m)}(\boldsymbol{\xi'}) \frac{Z_{3,ijk}(\boldsymbol{\xi},\boldsymbol{\xi'},t)}{Z_{2,ij}(\boldsymbol{\xi},t)} \,\mathrm{d}\boldsymbol{\xi'} + \omega_{ij}^{(m)}(\boldsymbol{\xi}), \tag{20}$$

$$P_{2,ij}(\boldsymbol{\xi},t) = p_i + \sum_k \int \omega_{ik}^{(p)}(\boldsymbol{\xi'}) \frac{Z_{3,ijk}(\boldsymbol{\xi},\boldsymbol{\xi'},t)}{Z_{2,ij}(\boldsymbol{\xi},t)} \,\mathrm{d}\boldsymbol{\xi'} + \omega_{ij}^{(p)}(\boldsymbol{\xi}). \tag{21}$$

The third term on the right of Equations (20)-(21) accounts for the direct influence of the agent of type $j$ at a displacement $\boldsymbol{\xi}$ from the agent of type $i$.

bioRxiv preprint doi: https://doi.org/10.1101/267708; this version posted February 18, 2018. The copyright holder for this preprint (which was not certified by peer review) is the author/funder. All rights reserved. No reuse allowed without permission.



The gradient of the interaction kernel gives the contribution of agents to the bias vector of the neighboring agent. The expected net bias vector of an agent of type $i$, conditional on presence of an agent of type $j$, is given by,

$$\boldsymbol{B}_{2,ij}(\boldsymbol{\xi},t) = \boldsymbol{b}_i + \sum_k \int \nabla\omega_{ik}^{(b)}(\boldsymbol{\xi}')\frac{Z_{3,ijk}(\boldsymbol{\xi},\boldsymbol{\xi}',t)}{Z_{2,ij}(\boldsymbol{\xi},t)}\,\mathrm{d}\boldsymbol{\xi}' + \nabla\omega_{ij}^{(b)}(\boldsymbol{\xi}). \tag{22}$$

Again, the third term on the right of Equation (22) accounts for the direct influence of the agent of type $j$, at a displacement $\boldsymbol{\xi}$, from the agent of type $i$. We note that Equation (22) combines directional bias (Binny et al. 2016a,2016b) with multi-species spatial moment equations (Law and Dieckmann 2000; Murrell 2005; Plank and Law 2015) in a way that has not been considered previously. Now we consider the probability of a motile agent of type $i$ moving a displacement $\boldsymbol{\xi}'$, conditional on the presence of a neighbor of type $j$ at displacement $\boldsymbol{\xi}$ as,

$$\mu_{2,ij}^{(m)}(\boldsymbol{\xi}',\boldsymbol{\xi},t) = \mu_{ij}^{(m)}(\boldsymbol{\xi}';B_{2,ij}(\boldsymbol{\xi},t)). \tag{23}$$

For the dynamics of the second moment, we must consider two factors which include the loss of pairs of agents at displacement $\boldsymbol{\xi}$, and the creation of pairs at displacement $\boldsymbol{\xi}$. The loss of pairs occurs either by movement or death events, whereas the creation of pairs occurs through movement or proliferation events. The time evolution of the second moment is given by,

$$\begin{aligned}\frac{\partial}{\partial t}Z_{2,ij}(\boldsymbol{\xi},t) = &-\Big(M_{2,ij}(\boldsymbol{\xi},t) + M_{2,ji}(-\boldsymbol{\xi},t) + d_i + d_j\Big)Z_{2,ij}(\boldsymbol{\xi},t)\\ &+\int\Big(\mu_{ij}^{(m)}(\boldsymbol{\xi}',\boldsymbol{\xi}'+\boldsymbol{\xi},t)M_{2,ij}(\boldsymbol{\xi}'+\boldsymbol{\xi},t)\\ &+\mu_i^{(p)}(\boldsymbol{\xi}')P_{2,ij}(\boldsymbol{\xi}'+\boldsymbol{\xi},t)\Big)Z_{2,ij}(\boldsymbol{\xi}'+\boldsymbol{\xi},t)\,\mathrm{d}\boldsymbol{\xi}'\\ &+\int\Big(\mu_{ji}^{(m)}(\boldsymbol{\xi}',\boldsymbol{\xi}'-\boldsymbol{\xi},t)M_{2,ji}(\boldsymbol{\xi}'-\boldsymbol{\xi},t)\\ &+\mu_j^{(p)}(\boldsymbol{\xi}')P_{2,ji}(\boldsymbol{\xi}'-\boldsymbol{\xi},t)\Big)Z_{2,ji}(\boldsymbol{\xi}'-\boldsymbol{\xi},t)\mathrm{d}\boldsymbol{\xi}'\\ &+2\delta_{ij}\mu_j^{(p)}(-\boldsymbol{\xi})P_{1,j}(t)Z_{1,j}(t).\end{aligned} \tag{24}$$

In Equation (24), the two integral terms and the factor of two in the last term on the right arises due to the fact that a pair can be created or destroyed by either of the individuals in that pair.

Just as the dynamics of the first moment depends on the second moment, we see that the dynamics of the second moment depends on the third moment. If we continue in this way we could develop an infinite hierarchy of moment equations which is difficult to analyze (Ovaskainen and Cornell 2006; Finkelshtein et al. 2009; Ovaskainen et al. 2014). However, previous studies focusing on applications in cell biology (Binny et al. 2016a,2016b) and ecology (Law and Dieckmann 2000) provide useful results by closing the infinite system of moment equations to produce a truncated system. Here we follow

bioRxiv preprint doi: https://doi.org/10.1101/267708; this version posted February 18, 2018. The copyright holder for this preprint (which was not certified by peer review) is the author/funder. All rights reserved. No reuse allowed without permission.



a similar approach and approximate the third order terms in Equations (20)-(22) using a moment closure approximation. While various approximations, such as the power-1 closure, power-2 closure and Kirkwood superposition approximation, are available (Murrell et al. 2004), in this study we focus on the power-2 closure scheme given by,

$$Z_{3,ijk}(\boldsymbol{\xi},\boldsymbol{\xi'},t) = \frac{1}{\alpha+\gamma}\Big(\alpha\frac{Z_{2,ij}(\boldsymbol{\xi},t)Z_{2,ik}(\boldsymbol{\xi'},t)}{Z_{1,i}(t)} + \beta\frac{Z_{2,ij}(\boldsymbol{\xi},t)Z_{2,jk}(\boldsymbol{\xi'}-\boldsymbol{\xi},t)}{Z_{1,j}(t)} + \gamma\frac{Z_{2,ik}(\boldsymbol{\xi'},t)Z_{2,jk}(\boldsymbol{\xi'}-\boldsymbol{\xi},t)}{Z_{1,k}(t)} - \beta Z_{1,i}(t)Z_{1,j}(t)Z_{1,k}(t)\Big), \quad (25)$$

which expresses the third moment in terms of the first and second moment. For all results presented here we choose the parameters $(\alpha,\beta,\gamma) = (4,1,1)$, which corresponds to the asymmetric power-2 closure as discussed by Law et al. (2003).

### 4.3 Spatial moment dynamics description for a population of motile, proliferative agents in an environment containing obstacles

For clarity, we will now present the governing equations for the specific case of a population of motile, proliferative agents in an environment containing stationary, non-proliferative obstacles. The first spatial moment of agents and obstacles are denoted $Z_{1,1}(t)$ and $Z_{1,2}(t)$, respectively. The second spatial moments, corresponding to the density of pairs are denoted: $Z_{2,11}(\boldsymbol{\xi},t)$; $Z_{2,12}(\boldsymbol{\xi},t)$; $Z_{2,21}(\boldsymbol{\xi},t)$; and $Z_{2,22}(\boldsymbol{\xi},t)$. The terms $Z_{2,11}(\boldsymbol{\xi},t)$ and $Z_{2,22}(\boldsymbol{\xi},t)$ correspond to the average densities agent-agent pairs and obstacle-obstacle pairs. The other two terms, $Z_{2,12}(\boldsymbol{\xi},t)$ and $Z_{2,21}(\boldsymbol{\xi},t)$, corresponds to the average densities of agent-obstacle pairs, and obstacle-agent pairs.

The expected rate of movement of an agent, $M_{1,1}(t)$, is given by multiplying the interaction kernels of movement, $\omega_{11}^{(m)}(\boldsymbol{\xi})$ or $\omega_{12}^{(m)}(\boldsymbol{\xi})$, by the conditional probability of having an agent or obstacle present at a displacement $\boldsymbol{\xi}$ from the reference agent, and integrating over all possible displacements. These conditional probabilities of either an agent or obstacle located at a displacement $\boldsymbol{\xi}$ are given by $Z_{2,11}(\boldsymbol{\xi},t)/Z_{1,1}(t)$ and $Z_{2,12}(\boldsymbol{\xi},t)/Z_{1,1}(t)$, respectively. The expected proliferation rate is also calculated in the same way by replacing the movement kernels with proliferation kernels, $\omega_{11}^{(p)}(\boldsymbol{\xi})$ and $\omega_{12}^{(p)}(\boldsymbol{\xi})$. Using this information, the expected rate of movement and proliferation of an agent is given by,

$$M_{1,1}(t) = m_1 + \frac{1}{Z_{1,1}(t)}\int\Big(\omega_{11}^{(m)}(\boldsymbol{\xi})Z_{2,11}(\boldsymbol{\xi},t) + \omega_{12}^{(m)}(\boldsymbol{\xi})Z_{2,12}(\boldsymbol{\xi},t)\Big)\,\mathrm{d}\boldsymbol{\xi}, \quad (26)$$

$$P_{1,1}(t) = p_1 + \frac{1}{Z_{1,1}(t)}\int\Big(\omega_{11}^{(p)}(\boldsymbol{\xi})Z_{2,11}(\boldsymbol{\xi},t) + \omega_{12}^{(p)}(\boldsymbol{\xi})Z_{2,12}(\boldsymbol{\xi},t)\Big)\,\mathrm{d}\boldsymbol{\xi}. \quad (27)$$

The expected movement and proliferation rates of obstacles $M_{1,2}(t)$ and $P_{1,2}(t)$ are zero, by definition.

bioRxiv preprint doi: https://doi.org/10.1101/267708; this version posted February 18, 2018. The copyright holder for this preprint (which was not certified by peer review) is the author/funder. All rights reserved. No reuse allowed without permission.



Now we derive the dynamics of the first moment. The time evolution of density of agents depends only on the expected rate of proliferation and death of agents. The density of obstacles remains constant. Hence we have,

$$\frac{\mathrm{d}}{\mathrm{d}t}Z_{1,1}(t) = (P_{1,1}(t) - d_1)Z_{1,1}(t), \tag{28}$$

$$\frac{\mathrm{d}}{\mathrm{d}t}Z_{1,2}(t) = 0. \tag{29}$$

The conditional probability of having an agent located at $\boldsymbol{\xi'}$, given that an another agent is present at $\boldsymbol{\xi}$, is $Z_{3,111}(\xi, \xi', t)/Z_{2,11}(\xi, t)$. Similarly three more conditional probabilities can be specified by considering different arrangements of agents and obstacles around the reference agent at displacement $\mathbf{0}$. The expected event rates, $M_{2,11}(\boldsymbol{\xi}, t)$ and $P_{2,11}(\boldsymbol{\xi}, t)$, of an agent conditional on the presence of another agent at displacement $\boldsymbol{\xi}$ can be computed by multiplying these conditional probabilities by the corresponding interaction kernels and integrating over all possible displacements. The expected rates are given by,

$$\begin{aligned} M_{2,11}(\boldsymbol{\xi}, t) =& \frac{1}{Z_{2,11}(\boldsymbol{\xi}, t)} \int \left(\omega_{11}^{(m)}(\boldsymbol{\xi'}) Z_{3,111}(\boldsymbol{\xi}, \boldsymbol{\xi'}, t) + \omega_{12}^{(m)}(\boldsymbol{\xi'}) Z_{3,112}(\boldsymbol{\xi}, \boldsymbol{\xi'}, t)\right) \mathrm{d}\boldsymbol{\xi'} \\ &+ m_1 + \omega_{11}^{(m)}(\boldsymbol{\xi}), \end{aligned} \tag{30}$$

$$\begin{aligned} P_{2,11}(\boldsymbol{\xi}, t) =& \frac{1}{Z_{2,11}(\boldsymbol{\xi}, t)} \int \left(\omega_{11}^{(p)}(\boldsymbol{\xi'}) Z_{3,111}(\boldsymbol{\xi}, \boldsymbol{\xi'}, t) + \omega_{12}^{(p)}(\boldsymbol{\xi'}) Z_{3,112}(\boldsymbol{\xi}, \boldsymbol{\xi'}, t)\right) \mathrm{d}\boldsymbol{\xi'} \\ &+ p_1 + \omega_{11}^{(p)}(\boldsymbol{\xi}). \end{aligned} \tag{31}$$

Using similar arguments, we compute the remaining movement and proliferation rates of an agent arising from the presence of an obstacle at a displacement $\boldsymbol{\xi}$ as follows,

$$\begin{aligned} M_{2,12}(\boldsymbol{\xi}, t) =& \frac{1}{Z_{2,12}(\boldsymbol{\xi}, t)} \int \left(\omega_{11}^{(m)}(\boldsymbol{\xi'}) Z_{3,121}(\boldsymbol{\xi}, \boldsymbol{\xi'}, t) + \omega_{12}^{(m)}(\boldsymbol{\xi'}) Z_{3,122}(\boldsymbol{\xi}, \boldsymbol{\xi'}, t)\right) \mathrm{d}\boldsymbol{\xi'} \\ &+ m_1 + \omega_{12}^{(m)}(\boldsymbol{\xi}), \end{aligned} \tag{32}$$

$$\begin{aligned} P_{2,12}(\boldsymbol{\xi}, t) =& \frac{1}{Z_{2,12}(\boldsymbol{\xi}, t)} \int \left(\omega_{11}^{(p)}(\boldsymbol{\xi'}) Z_{3,121}(\boldsymbol{\xi}, \boldsymbol{\xi'}, t) + \omega_{12}^{(p)}(\boldsymbol{\xi'}) Z_{3,122}(\boldsymbol{\xi}, \boldsymbol{\xi'}, t)\right) \mathrm{d}\boldsymbol{\xi'} \\ &+ p_1 + \omega_{12}^{(p)}(\boldsymbol{\xi}). \end{aligned} \tag{33}$$

The gradient of the bias kernel gives the contribution of agents and obstacles to the bias vector of the neighboring agent. The expected net bias vector of an agent conditional on presence of another agent is given by,

$$\begin{aligned} \mathbf{B}_{2,11}(\boldsymbol{\xi}, t) =& \mathbf{b}_1 + \frac{1}{Z_{2,11}(\boldsymbol{\xi}, t)} \int \left(\nabla\omega_{11}^{(b)}(\boldsymbol{\xi'}) Z_{3,111}(\boldsymbol{\xi}, \boldsymbol{\xi'}, t)\right. \\ &\left. + \nabla\omega_{12}^{(b)}(\boldsymbol{\xi'}) Z_{3,112}(\boldsymbol{\xi}, \boldsymbol{\xi'}, t)\right) \mathrm{d}\boldsymbol{\xi'} + \nabla\omega_{11}^{(b)}(\boldsymbol{\xi}). \end{aligned} \tag{34}$$

bioRxiv preprint doi: https://doi.org/10.1101/267708; this version posted February 18, 2018. The copyright holder for this preprint (which was not certified by peer review) is the author/funder. All rights reserved. No reuse allowed without permission.



Similarly, the expected net bias vector of an agent conditional on presence of an obstacle is given by,

$$\begin{aligned}\mathbf{B}_{2,12}(\boldsymbol{\xi},t) = \mathbf{b}_1 + \frac{1}{Z_{2,12}(\boldsymbol{\xi},t)}\int \Big(&\nabla\omega_{11}^{(b)}(\boldsymbol{\xi}')Z_{3,121}(\boldsymbol{\xi},\boldsymbol{\xi}',t)\\ &+\nabla\omega_{12}^{(b)}(\boldsymbol{\xi}')Z_{3,122}(\boldsymbol{\xi},\boldsymbol{\xi}',t)\Big)\,\mathrm{d}\boldsymbol{\xi}' + \nabla\omega_{12}^{(b)}(\boldsymbol{\xi}).\end{aligned} \tag{35}$$

Now we develop the equations governing the dynamics of the second moments. The equations for the density of pairs involving agents depends on the loss of pairs of agents at displacement $\boldsymbol{\xi}$, which can occur either by movement or death, and creation of pair at displacement $\boldsymbol{\xi}$ which can occur through movement or proliferation. The density of pairs of obstacles, $Z_{2,22}(\boldsymbol{\xi},t)$, remains constant over time. Now the equations governing the dynamics of second moments for agent-obstacle population are given by,

$$\begin{aligned}\frac{\partial}{\partial t}Z_{2,11}(\boldsymbol{\xi},t) =& -\Big(M_{2,11}(\boldsymbol{\xi},t) + M_{2,11}(-\boldsymbol{\xi},t) + 2d_1\Big)Z_{2,11}(\boldsymbol{\xi},t)\\ &+\int\Big(\mu_{11}^{(m)}(\boldsymbol{\xi}',\boldsymbol{\xi}'+\boldsymbol{\xi},t)M_{2,11}(\boldsymbol{\xi}'+\boldsymbol{\xi},t)\\ &+\mu_1^{(p)}(\boldsymbol{\xi}')P_{2,11}(\boldsymbol{\xi}'+\boldsymbol{\xi},t)\Big)Z_{2,11}(\boldsymbol{\xi}'+\boldsymbol{\xi},t)\,\mathrm{d}\boldsymbol{\xi}'\\ &+\int\Big(\mu_{11}^{(m)}(\boldsymbol{\xi}',\boldsymbol{\xi}'-\boldsymbol{\xi},t)M_{2,11}(\boldsymbol{\xi}'-\boldsymbol{\xi},t)\\ &+\mu_1^{(p)}(\boldsymbol{\xi}')P_{2,11}(\boldsymbol{\xi}'-\boldsymbol{\xi},t)\Big)Z_{2,11}(\boldsymbol{\xi}'-\boldsymbol{\xi},t)\,\mathrm{d}\boldsymbol{\xi}'\\ &+2\mu_1^{(p)}(-\boldsymbol{\xi})P_{1,1}(t)Z_{1,1}(t),\end{aligned} \tag{36}$$

$$\begin{aligned}\frac{\partial}{\partial t}Z_{2,12}(\boldsymbol{\xi},t) =& -\Big(M_{2,12}(\boldsymbol{\xi},t) + d_1\Big)Z_{2,12}(\boldsymbol{\xi},t)\\ &+\int\Big(\mu_{12}^{(m)}(\boldsymbol{\xi}',\boldsymbol{\xi}'+\boldsymbol{\xi},t)M_{2,12}(\boldsymbol{\xi}'+\boldsymbol{\xi},t)\\ &+\mu_1^{(p)}(\boldsymbol{\xi}')P_{2,12}(\boldsymbol{\xi}'+\boldsymbol{\xi},t)\Big)Z_{2,12}(\boldsymbol{\xi}'+\boldsymbol{\xi},t)\,\mathrm{d}\boldsymbol{\xi}',\end{aligned} \tag{37}$$

$$\begin{aligned}\frac{\partial}{\partial t}Z_{2,21}(\boldsymbol{\xi},t) =& -\Big(M_{2,12}(-\boldsymbol{\xi},t) + d_1\Big)Z_{2,21}(\boldsymbol{\xi},t)\\ &+\int\Big(\mu_{12}^{(m)}(\boldsymbol{\xi}',\boldsymbol{\xi}'-\boldsymbol{\xi},t)M_{2,12}(\boldsymbol{\xi}'-\boldsymbol{\xi},t)\\ &+\mu_1^{(p)}(\boldsymbol{\xi}')P_{2,12}(\boldsymbol{\xi}'-\boldsymbol{\xi},t)\Big)Z_{2,12}(\boldsymbol{\xi}'-\boldsymbol{\xi},t)\,\mathrm{d}\boldsymbol{\xi}',\end{aligned} \tag{38}$$

$$\frac{\partial}{\partial t}Z_{2,22}(\boldsymbol{\xi},t) = 0. \tag{39}$$

### 4.4 Numerical methods

The system of equations governing the dynamics of the second spatial moments, Equations (36)-(39) are solved numerically using the forward Euler

bioRxiv preprint doi: https://doi.org/10.1101/267708; this version posted February 18, 2018. The copyright holder for this preprint (which was not certified by peer review) is the author/funder. All rights reserved. No reuse allowed without permission.



method. The numerical scheme involves spatially discretizing the displacement, $\boldsymbol{\xi} = (\xi_x, \xi_y)$, over the domain $\{-\xi_{\max} \leq \xi_x, \xi_y \leq \xi_{\max}\}$, with a grid spacing $\Delta\xi$. In all cases we have $\Delta\xi = 0.2$, and our calculations show that this choice is sufficient to produce grid-independent results. We choose $\xi_{\max}$ to be sufficiently large so that $Z_{2,ij}(\boldsymbol{\xi}, t) \approx Z_{1,i}(t) \times Z_{1,j}(t)$ at the boundary. The integral terms in Equations (26)-(27) and Equations (30)-(39) are approximated using the trapezoid rule. To evaluate the integrals we need the values of $Z_{2,ij}(\boldsymbol{\xi} + \boldsymbol{\xi}', t)$. For sufficiently large $\boldsymbol{\xi}$ and $\boldsymbol{\xi}'$, these values will lie outside of the computational domain. In that case, we replace those terms with the value of $Z_{2,ij}(\boldsymbol{\xi}, t)$ at the boundary, $Z_{2,ij}((\xi_{\max}, \xi_{\max}), t)$. The movement and dispersal PDFs are normalized using the trapezoid rule with the same spatial discretization such that $\int \mu_{ij}^{(m)}(\boldsymbol{\xi}, \boldsymbol{\xi}')\mathrm{d}\boldsymbol{\xi} = 1$ and $\int \mu_i^{(p)}(\boldsymbol{\xi})\mathrm{d}\boldsymbol{\xi} = 1$, for a fixed value of $\boldsymbol{\xi}'$.

To solve the system of equations corresponding to the second spatial moments, Equations (36)-(39), we also need the values of $Z_{1,1}(t)$ and $Z_{1,2}(t)$. The large computational domain, together with the fact that we only consider local interactions, means that the usual mean-field condition will hold at large displacements. This means that we can evaluate the first moments without solving the Equations (28)-(29). At each time step, we use values of $Z_{2,11}(\boldsymbol{\xi}, t)$ and $Z_{2,22}(\boldsymbol{\xi}, t)$ at the boundary to compute the first moments since we have $Z_{1,1}(t) = \sqrt{Z_{2,11}((\xi_{\max}, \xi_{\max}), t)}$ and $Z_{1,2}(t) = \sqrt{Z_{2,22}((\xi_{\max}, \xi_{\max}), t)}$, respectively. To compare predictions from the spatial moment model with results from the IBM, we compute auto-correlation and cross-correlation PCFs as $Z_{2,11}(\boldsymbol{\xi}, t)/Z_{1,1}(t)$ and $Z_{2,12}(\boldsymbol{\xi}, t)/(Z_{1,1}(t)Z_{1,2}(t))$, respectively. The initial condition used in solving the dynamics of the second spatial moment is $Z_{2,ij}(\boldsymbol{\xi}, 0) = Z_{1,i}(0)Z_{1,j}(0)$ at $t = 0$. For all results we set the time step to be $\mathrm{d}t = 0.1$, which is sufficiently small so that our numerical solutions are insensitive to this choice.

## 5 Results and discussion

In this section we present snapshots from the IBM to explore the dynamics of the two species agent-obstacle system. In these simulations we systematically vary the density of obstacles, the size of obstacles, and the interactions between agents and obstacles. In addition to presenting IBM simulations, we also present solutions of the spatial moment dynamics model to explore how well the model predicts the dynamics of the different conditions we consider. Another outcome is to examine how various properties of obstacle field influence spatial structure.

### 5.1 Effect of varying the obstacle density

Here we first explore how variations in the density of obstacles affects the spatial structure and the dynamics of the agent subpopulation. Results in

bioRxiv preprint doi: https://doi.org/10.1101/267708; this version posted February 18, 2018. The copyright holder for this preprint (which was not certified by peer review) is the author/funder. All rights reserved. No reuse allowed without permission.



Figure 3 show a series of snapshots from the IBM. Each row shows snapshots at $t = 0, 10, 20$ and 60, whereas each column shows results for different densities of obstacles. The initial number of obstacles is varied from $N_2(0) = 0$, 50, 100 to 150, in the columns from left-to-right, respectively. In all cases we consider a constant initial number of agents, $N_1(0) = 100$, and a random initial placement of obstacles and agents. Results in Figure 3(a)-(d) show the most fundamental case where there are no obstacles present, and we note that the multi-species model simplifies to the previous single species model presented by Binny et al. (2016b) in this case. We use this first scenario to emphasise the differences in the population dynamics for the agent subpopulation in presence and absence of obstacles, which are shown in the second, third and fourth column of Figure 3. By repeating the stochastic simulations in Figure 3 many times, we can calculate the density of obstacles, the density of agents, the auto-correlation PCF and the cross-correlation PCF, as shown in Figure 4.

bioRxiv preprint doi: https://doi.org/10.1101/267708; this version posted February 18, 2018. The copyright holder for this preprint (which was not certified by peer review) is the author/funder. All rights reserved. No reuse allowed without permission.



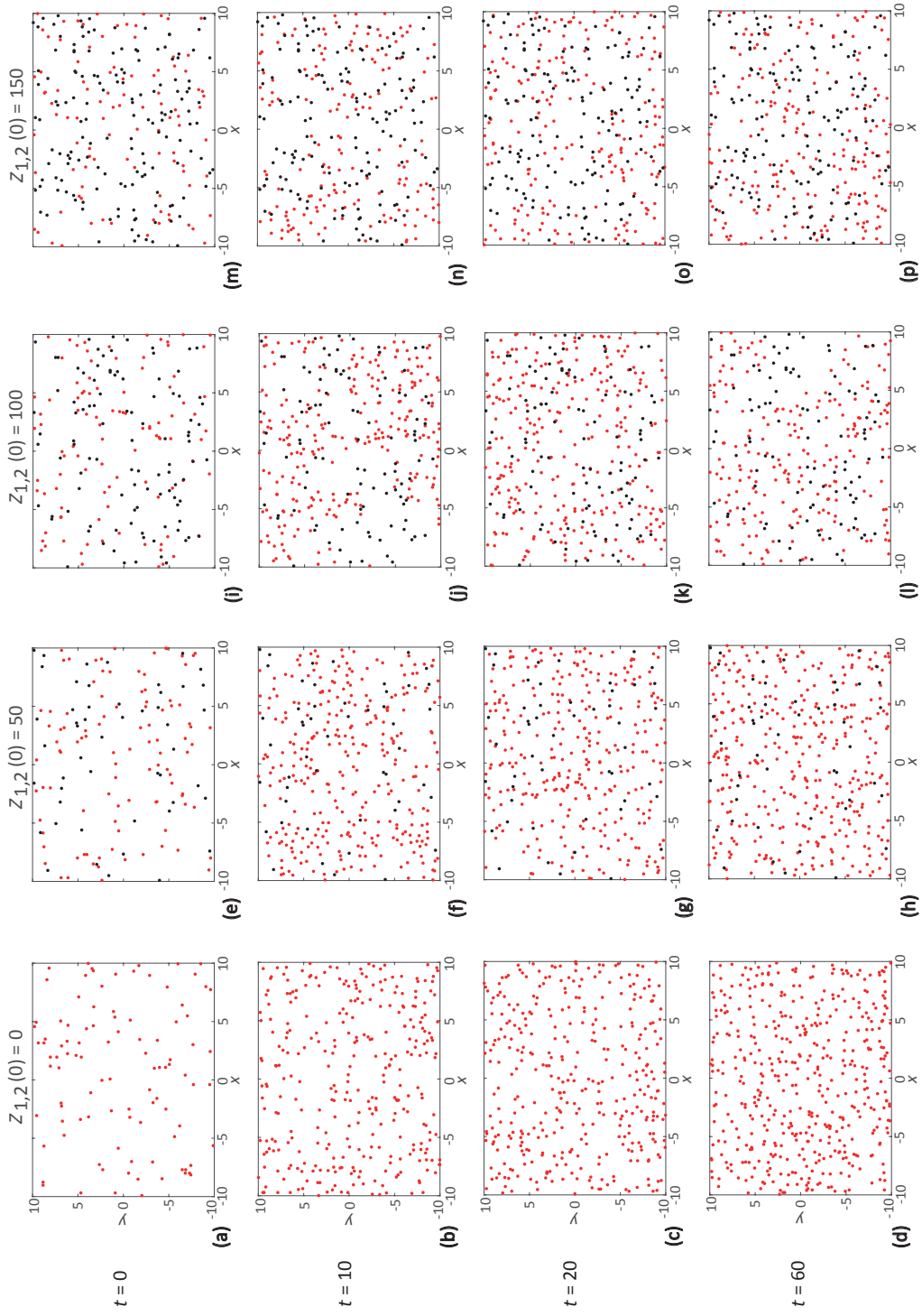


**Fig. 3** IBM snapshots showing the impact of increasing obstacle density. Each row shows a snapshot of the IBM at $t = 0$, 10, 20 and 60, respectively. Results in **a-d** show the evolution of a population of agents in the absence of obstacles. Results in **e-h**, **i-l** and **m-p** show the evolution of a population of agents among a population of 50, 100 and 150 obstacles, respectively. In all cases agents are red and obstacles are black. Parameter values are $p_1 = 1$, $d_1 = 0.5$, $m_1 = 5$, $p_2 = d_2 = m_2 = 0$, $\gamma_{11}^{(p)} = 0$, $\gamma_{12}^{(p)} = -0.38$, $\gamma_{21}^{(p)} = \gamma_{22}^{(p)} = 0$, $\gamma_{11}^{(b)} = 0.1$, $\gamma_{12}^{(b)} = 0.1$, $\gamma_{21}^{(b)} = \gamma_{22}^{(b)} = 0$, $\gamma_{11}^{(m)} = \gamma_{12}^{(m)} = \gamma_{21}^{(m)} = \gamma_{22}^{(m)} = 0$, $\sigma_{11}^{(p)} = 0.5$, $\sigma_{12}^{(p)} = 0.5$, $\sigma_{21}^{(p)} = 0.5$, $\sigma_{22}^{(p)} = 0.5$, $\sigma_{11}^{(b)} = 0.5$, $\sigma_{12}^{(b)} = 0.5$, $\sigma_{21}^{(b)} = 0.5$, $\sigma_{22}^{(b)} = 0.5$, $\sigma_{11}^{(m)} = 0.5$, $\sigma_{12}^{(m)} = 0.5$, $\sigma_{21}^{(m)} = 0.5$, $\sigma_{22}^{(m)} = 0.5$, $\mu_1^{(s)} = 0.4$, $\mu_2^{(s)} = 0.4$, $\sigma_1^{(s)} = 0.1$, $\sigma_2^{(s)} = 0.1$, $\sigma_1^{(d)} = 0.5$, and $\sigma_2^{(d)} = 0.5$.

bioRxiv preprint doi: https://doi.org/10.1101/267708; this version posted February 18, 2018. The copyright holder for this preprint (which was not certified by peer review) is the author/funder. All rights reserved. No reuse allowed without permission.



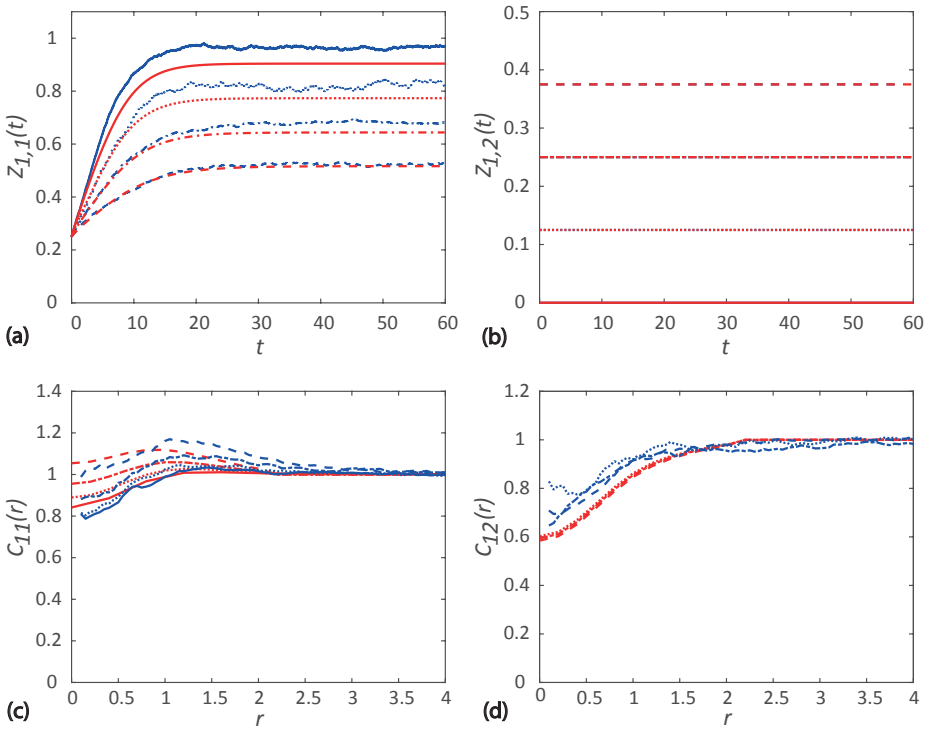


**Fig. 4** Comparison of spatial moment results and averaged data from 40 identically-prepared realizations of the IBM. Results in **a** show the evolution of the first spatial moment for the agents, $Z_{1,1}(t)$. Various results are superimposed for different obstacle densities of obstacles: $Z_{1,2}(0) = 0/400$ (solid), $Z_{1,2}(0) = 50/400$ (dotted), $Z_{1,2}(0) = 100/400$ (dash-dotted) and $Z_{1,2}(0) = 150/400$ (dashed). Results in **b** show the constant first spatial moment for the obstacles. Results in **c-d** show the second spatial moment of agents expressed in terms of $C_{11}(r)$ and $C_{12}(r)$, respectively. Both PCFs are given at $t = 60$. The curves in red correspond to results from the spatial moment dynamics model, whereas curves in blue correspond to averaged data from the IBM. Parameter values are $p_1 = 1$, $d_1 = 0.5$, $m_1 = 5$, $p_2 = d_2 = m_2 = 0$, $\gamma_{11}^{(p)} = -0.38$, $\gamma_{12}^{(p)} = -0.38$, $\gamma_{21}^{(p)} = \gamma_{22}^{(p)} = 0$, $\gamma_{11}^{(b)} = 0.1$, $\gamma_{12}^{(b)} = 0.1$, $\gamma_{21}^{(b)} = \gamma_{22}^{(b)} = 0$, $\gamma_{11}^{(m)} = \gamma_{12}^{(m)} = \gamma_{21}^{(m)} = \gamma_{22}^{(m)} = 0$, $\sigma_{11}^{(p)} = 0.5$, $\sigma_{12}^{(p)} = 0.5$, $\sigma_{21}^{(p)} = 0.5$, $\sigma_{22}^{(p)} = 0.5$, $\sigma_{11}^{(b)} = 0.5$, $\sigma_{12}^{(b)} = 0.5$, $\sigma_{21}^{(b)} = 0.5$, $\sigma_{22}^{(b)} = 0.5$, $\sigma_{11}^{(m)} = 0.5$, $\sigma_{12}^{(m)} = 0.5$, $\sigma_{21}^{(m)} = 0.5$, $\sigma_{22}^{(m)} = 0.5$, $\mu_1^{(s)} = 0.4$, $\mu_2^{(s)} = 0.4$, $\sigma_1^{(s)} = 0.1$, $\sigma_2^{(s)} = 0.1$, $\sigma_1^{(d)} = 0.5$, and $\sigma_2^{(d)} = 0.5$.

bioRxiv preprint doi: https://doi.org/10.1101/267708; this version posted February 18, 2018. The copyright holder for this preprint (which was not certified by peer review) is the author/funder. All rights reserved. No reuse allowed without permission.



Results in Figure 3(a)-(d) show the evolution of the population of agents and the associated spatial structure in the absence of obstacles. Overall we see that the initially small population of agents increases with time until there is a balance of net proliferation and death, leading to the formation of a steady density of agents at later time. For this choice of parameters we observe the formation of a segregated spatial pattern. The main reason for the emergence of the segregation pattern is the choice of a positive bias strength, $\gamma_{11}^{(b)} > 0$ which means that agents tend to move away from regions of high density. The segregated nature of the distribution of agents is evident in the auto-correlation PCF as we see that $C_{11}(r) < 1$ over relatively short distances, $r$.

The incorporation of obstacles in the system leads to a reduction in the long time steady density of agents, as shown in Figure 4(a). In general we see that the more obstacles present, the smaller the steady state density of agents. This results makes intuitive sense as the presence of obstacles in the system increases the role of agent-obstacle interactions, which acts to reduce the net proliferation rate. Results in Figure 4(b) show the time evolution of density of obstacles and we see the expected result that the density remains constant. However, the presence of obstacles influences the spatial structure of the population of agents by contributing to the directional bias. Since the obstacles are stationary, the obstacles prevent agents residing in certain regions of the domain. As we increase the obstacle density, we observe a progressive shift from the long time segregation of agents over short distances when there are no obstacles present, to a more clustered long time pattern of agents as the obstacle density increases. The auto-correlation PCF for each of the cases shown in Figure 4(c) illustrates this transition. The cross-correlation PCF between agents and obstacles appears to be less sensitive to the density of obstacles than the auto-correlation PCF. For all cases we see that $C_{12}(r) < 1$ over relatively short distances, $r$, for all the cases considered, indicating segregation of agents and obstacles.

### 5.2 Effect of varying the obstacle size

Next we explore how variations in obstacle size affects the spatial structure and dynamics of the agent subpopulation. The notion of obstacle size is incorporated into the model by varying the spatial extent of the interaction of obstacles, $\sigma_{12}^{(p)}$ and $\sigma_{12}^{(b)}$. We assume that larger obstacles interact with agents over a greater distance than smaller obstacles. Therefore, we vary the size of the obstacles and examine how this impacts the evolution of the density of agents, and the spatial structure. We consider a total population composed of agents and obstacles with initial population sizes, $N_1(0) = N_2(0) = 100$, respectively, as shown in Figure 5. We then consider increasing the obstacle size, shown from left-to-right in Figure 5, where we have $\sigma_{12}^{(p)} = \sigma_{12}^{(b)} = 0.25$, 0.4, 0.5, and 0.6, respectively. By repeating the stochastic simulations in Figure 5 many times, we can calculate the density of obstacles, the density of agents,

bioRxiv preprint doi: https://doi.org/10.1101/267708; this version posted February 18, 2018. The copyright holder for this preprint (which was not certified by peer review) is the author/funder. All rights reserved. No reuse allowed without permission.



the auto-correlation PCF and the cross-correlation PCF, as shown in Figure 6.

bioRxiv preprint doi: https://doi.org/10.1101/267708; this version posted February 18, 2018. The copyright holder for this preprint (which was not certified by peer review) is the author/funder. All rights reserved. No reuse allowed without permission.



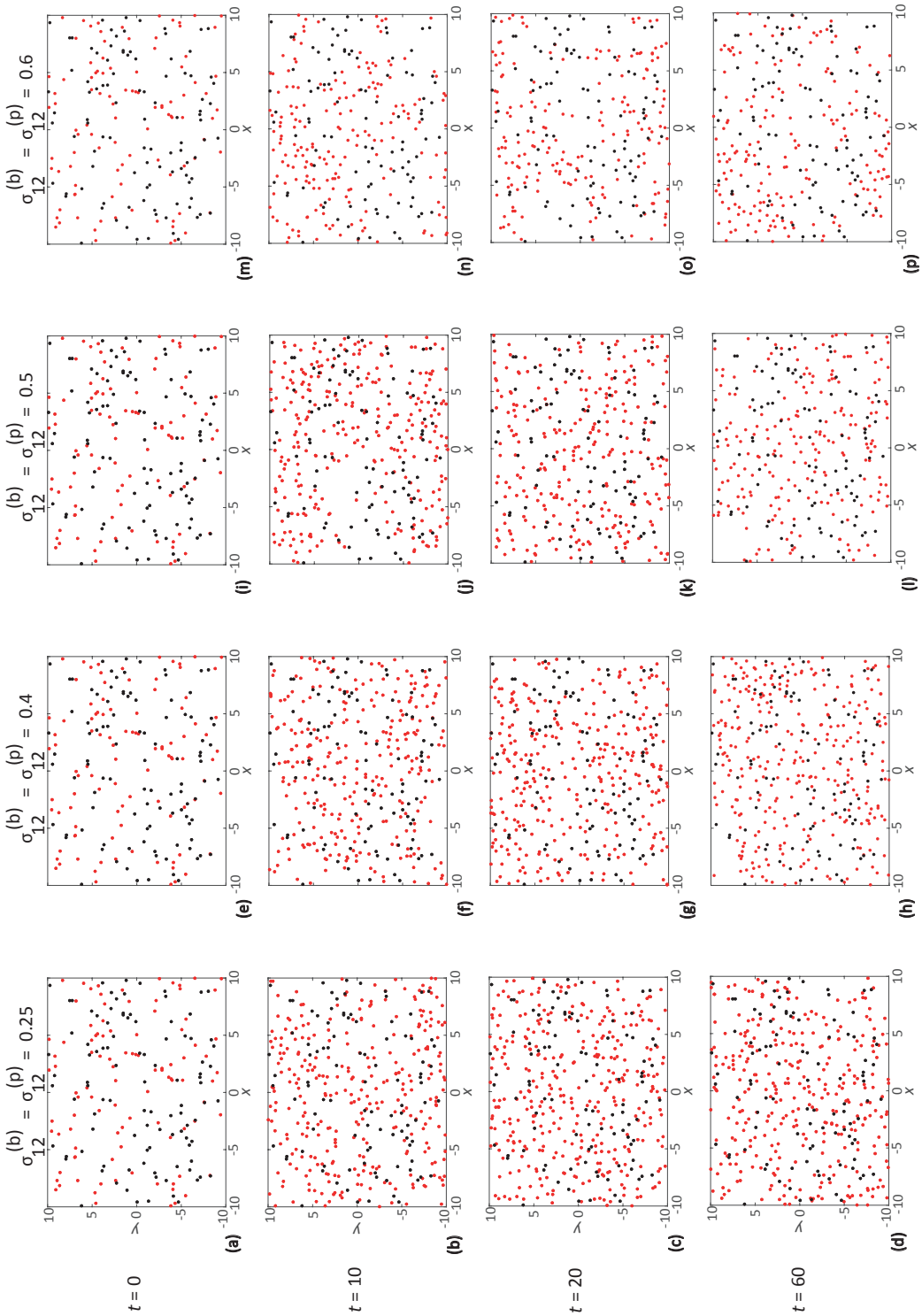


**Fig. 5** IBM snapshots showing the impact of increasing obstacle size. Each row shows a snapshot of the IBM at $t = 0$, 10, 20 and 60, respectively. Results in **a-d**, **e-h**, **i-l** and **m-p** show the evolution of a population of agents where $\sigma_{12}^{(p)} = \sigma_{12}^{(b)} = 0.25$; $\sigma_{12}^{(p)} = \sigma_{12}^{(b)} = 0.40$; $\sigma_{12}^{(p)} = \sigma_{12}^{(b)} = 0.50$; and $\sigma_{12}^{(p)} = \sigma_{12}^{(b)} = 0.60$, respectively. In each case the initial number of obstacles is 100. In all cases agents are red and obstacles are black. Parameter values are $p_1 = 1$, $d_1 = 0.5$, $m_1 = 5$, $p_2 = d_2 = m_2 = 0$, $\gamma_{11}^{(p)} = -0.38$, $\gamma_{12}^{(p)} = -0.38$, $\gamma_{21}^{(p)} = \gamma_{22}^{(p)} = 0$, $\gamma_{11}^{(b)} = 0.1$, $\gamma_{12}^{(b)} = 0.1$, $\gamma_{21}^{(b)} = \gamma_{22}^{(b)} = 0$, $\gamma_{11}^{(m)} = \gamma_{12}^{(m)} = \gamma_{21}^{(m)} = \gamma_{22}^{(m)} = 0$, $\sigma_{11}^{(p)} = 0.5$, $\sigma_{11}^{(b)} = 0.5$, $\sigma_{11}^{(m)} = 0.5$, $\mu_1^{(s)} = 0.4$, $\mu_2^{(s)} = 0.4$, $\sigma_1^{(s)} = 0.1$, $\sigma_2^{(s)} = 0.1$, $\sigma_1^{(d)} = 0.5$, and $\sigma_2^{(d)} = 0.5$

bioRxiv preprint doi: https://doi.org/10.1101/267708; this version posted February 18, 2018. The copyright holder for this preprint (which was not certified by peer review) is the author/funder. All rights reserved. No reuse allowed without permission.



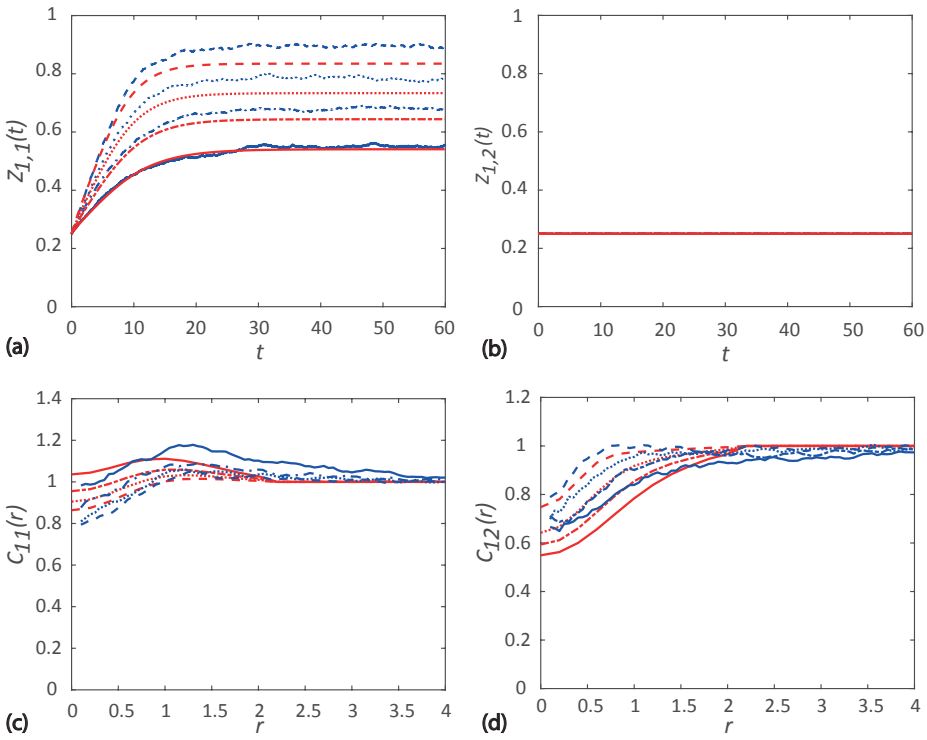


**Fig. 6** Comparison of spatial moment results and averaged data from 40 identically-prepared realizations of the IBM. Results in **a** show the evolution of the first spatial moment for agents, $Z_{1,1}(t)$. Various results are superimposed for different obstacle size: $\sigma_{12}^{(p)} = \sigma_{12}^{(b)} = 0.25$ (dashed); $\sigma_{12}^{(p)} = \sigma_{12}^{(b)} = 0.40$ (dotted); $\sigma_{12}^{(p)} = \sigma_{12}^{(b)} = 0.50$ (dash-dotted); and $\sigma_{12}^{(p)} = \sigma_{12}^{(b)} = 0.60$ (solid). Results in **b** show the constant first spatial moment for the obstacles. Results in **c-d** show the second spatial moment of agents expressed in terms of $C_{11}(r)$ and $C_{12}(r)$, respectively. Both PCFs are given at $t = 60$. **d** The curves in red correspond to results from the spatial moment dynamics model, whereas curves in blue correspond to averaged data from the IBM. Parameter values are $p_1 = 1$, $d_1 = 0.5$, $m_1 = 5$, $p_2 = d_2 = m_2 = 0$, $\gamma_{11}^{(p)} = -0.38$, $\gamma_{12}^{(p)} = -0.38$, $\gamma_{21}^{(p)} = \gamma_{22}^{(p)} = 0$, $\gamma_{11}^{(b)} = 0.1$, $\gamma_{12}^{(b)} = 0.1$, $\gamma_{21}^{(b)} = \gamma_{22}^{(b)} = 0$, $\gamma_{11}^{(m)} = \gamma_{12}^{(m)} = \gamma_{21}^{(m)} = \gamma_{22}^{(m)} = 0$, $\sigma_{11}^{(p)} = 0.5$, $\sigma_{11}^{(b)} = 0.5$, $\sigma_{11}^{(m)} = 0.5$, $\mu_1^{(s)} = 0.4$, $\mu_2^{(s)} = 0.4$, $\sigma_1^{(s)} = 0.1$, $\sigma_2^{(s)} = 0.1$, $\sigma_1^{(d)} = 0.5$, and $\sigma_2^{(d)} = 0.5$.

bioRxiv preprint doi: https://doi.org/10.1101/267708; this version posted February 18, 2018. The copyright holder for this preprint (which was not certified by peer review) is the author/funder. All rights reserved. No reuse allowed without permission.



Results in Figure 6(a)-(b) show the time evolution of the density of agents and the density of obstacles in each of the four cases considered. As the size of obstacles increase, we observe a decrease in the long time steady agent density. The wider range of interactions for the larger obstacles enables them to influence the proliferation rate of more distant agents. Even though the obstacle density is same, the proliferation rate of more agents reduces in the presence of large obstacles, leading to a reduced long time density of agents.

Figure 5 shows the snapshot of the spatial structure of population for each case considered and corresponding auto-correlation and cross-correlation PCFs are given in Figure 6(c)-(d). The population consisting of small obstacles shows a small-scale segregated spatial pattern of agents. Due to the narrow interaction range of the smaller obstacles, a relatively small number of agents are affected by the obstacles. However, the agents are also subject to a repulsive bias from other agents, which results in a small scale spatial segregation of agents for this choice of parameters. The cross-correlation PCF is less than unity over short displacements, thereby suggesting some segregation between agents and obstacles, but the effects are less pronounced than the segregation between agents. As the obstacle size increases, the agent population became less segregated, and the case we consider with the largest, $\sigma_{12}^{(p)} = 0.6$, leads to agent clustering over short distances.

### 5.3 Effect of varying the obstacle interaction strength

Finally, we explore how variations in interaction strength, and the nature of the interactions between agents and obstacles, affects the spatial structure and the dynamics of the agent population. We examine the influence of both attractive interactions, as well as repulsive interactions. Similar to the previous simulations in Figure 5, we consider a random initial spatial distribution of agents and obstacles with initial population size $N_1(0) = N_2(0) = 100$. We then vary the strength of interactions, $\gamma_{12}^{(b)}$, between 0.4 and -0.2. This means that we consider both attractive and repulsive interactions between agents and obstacles in this suite of simulations. Snapshots from the IBM are shown in Figure 7, and by repeating these stochastic simulations many times, we can calculate the density of obstacles, the density of agents, the auto-correlation PCF and the cross-correlation PCF, as shown in 8.

bioRxiv preprint doi: https://doi.org/10.1101/267708; this version posted February 18, 2018. The copyright holder for this preprint (which was not certified by peer review) is the author/funder. All rights reserved. No reuse allowed without permission.



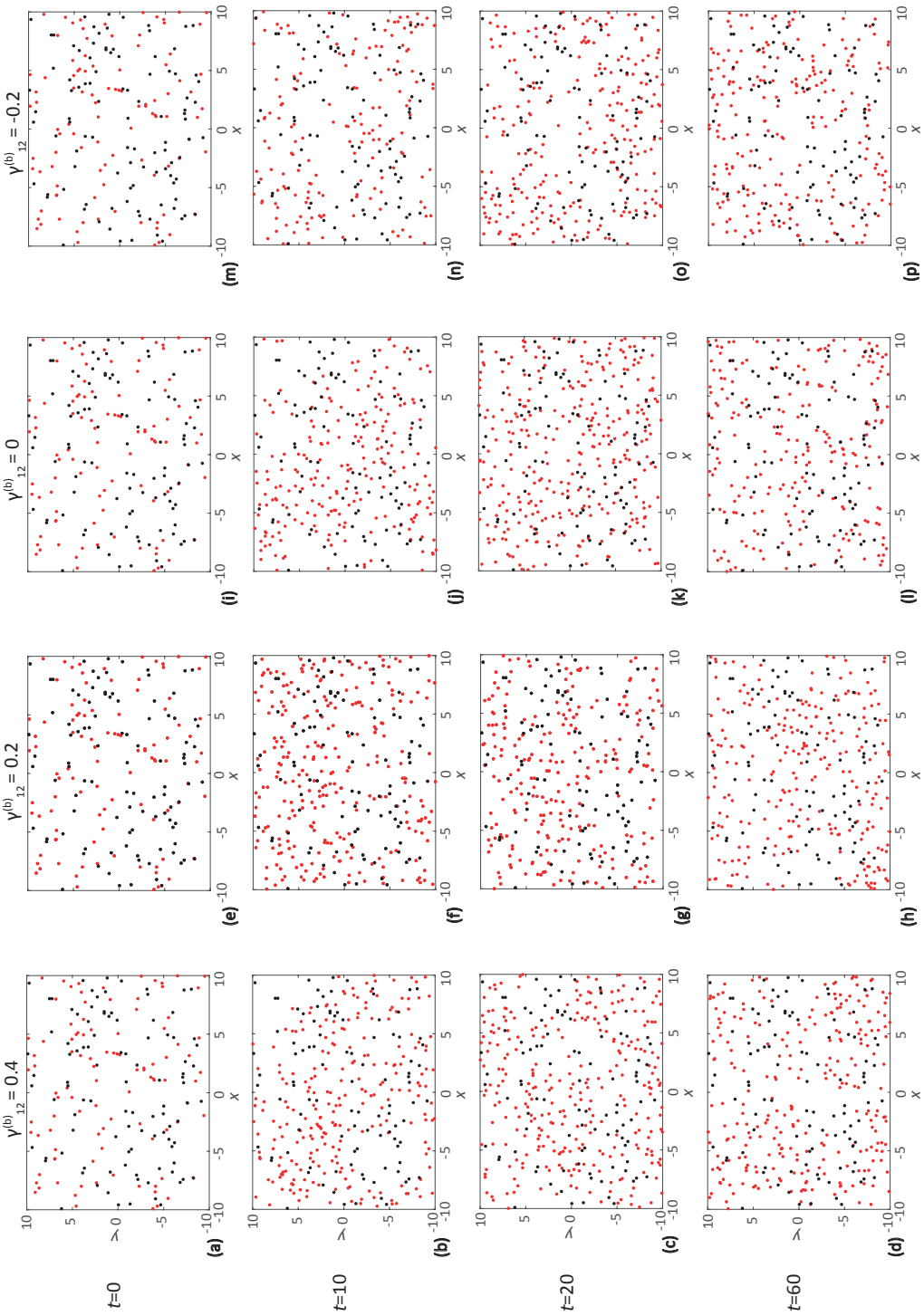


**Fig. 7** IBM snapshots showing the impact of increasing obstacle size. Each row shows a snapshot of the IBM at $t = 0$, 10, 20 and 60, respectively. , **e-h**, **i-l** and **m-p** show the evolution of a population of agents where $\gamma_{12}^{(b)} = 0.4$; $\gamma_{12}^{(b)} = 0.2$; $\gamma_{12}^{(b)} = 0.0$; and $\gamma_{12}^{(b)} = -0.2$, respectively. In each case the initial number of obstacles is 100. In all cases agents are red and obstacles are black. Parameter values are $p_1 = 1$, $d_1 = 0.5$, $m_1 = 5$, $p_2 = d_2 = m_2 = 0$, $\gamma_{11}^{(p)} = -0.38$, $\gamma_{12}^{(p)} = -0.38$, $\gamma_{21}^{(p)} = \gamma_{22}^{(p)} = 0$, $\gamma_{11}^{(b)} = 0.1$, $\gamma_{21}^{(b)} = \gamma_{22}^{(b)} = 0$, $\gamma_{11}^{(m)} = \gamma_{12}^{(m)} = \gamma_{21}^{(m)} = \gamma_{22}^{(m)} = 0$, $\sigma_{11}^{(p)} = 0.5$, $\sigma_{12}^{(p)} = 0.5$, $\sigma_{21}^{(p)} = 0.5$, $\sigma_{22}^{(p)} = 0.5$, $\sigma_{11}^{(b)} = 0.5$, $\sigma_{12}^{(b)} = 0.5$, $\sigma_{21}^{(b)} = 0.5$, $\sigma_{22}^{(b)} = 0.5$, $\sigma_{11}^{(m)} = 0.5$, $\sigma_{12}^{(m)} = 0.5$, $\sigma_{21}^{(m)} = 0.5$, $\sigma_{22}^{(m)} = 0.5$, $\mu_1^{(s)} = 0.4$, $\mu_2^{(s)} = 0.4$, $\sigma_1^{(s)} = 0.1$, $\sigma_2^{(s)} = 0.1$, $\sigma_1^{(d)} = 0.5$, and $\sigma_2^{(d)} = 0.5$.

bioRxiv preprint doi: https://doi.org/10.1101/267708; this version posted February 18, 2018. The copyright holder for this preprint (which was not certified by peer review) is the author/funder. All rights reserved. No reuse allowed without permission.



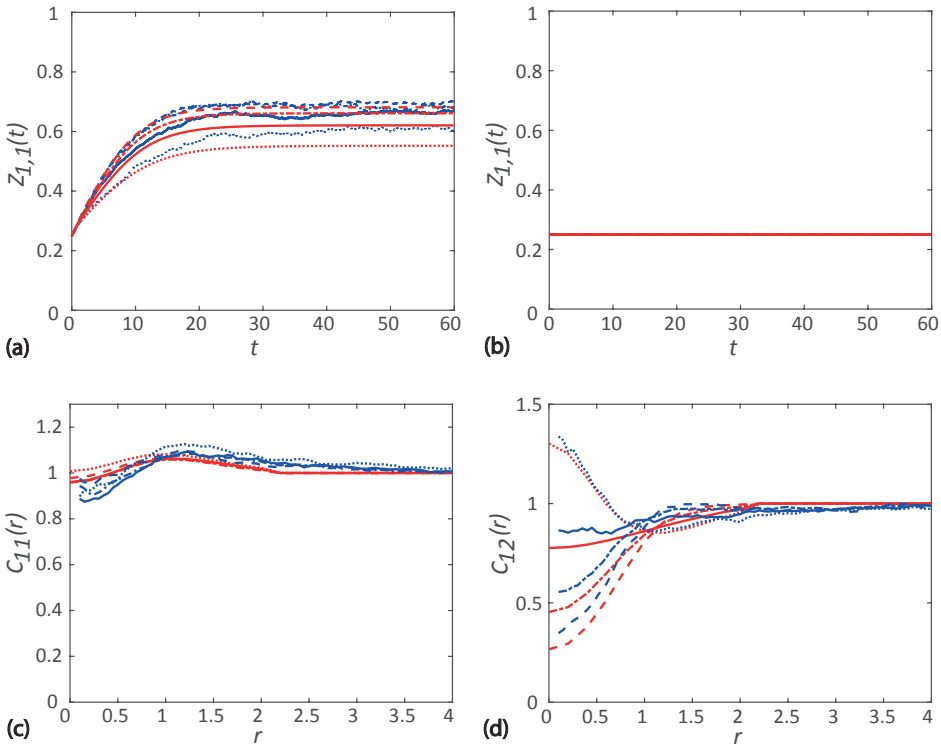


**Fig. 8** Comparison of spatial moment results and averaged data from 40 identically-prepared realizations of the IBM. Results in **a** show the evolution of the first spatial moment for agents, $Z_{1,1}(t)$. Various results are superimposed for different obstacle size: $\gamma_{12}^{(b)} = 0.4$ (dashed); $\gamma_{12}^{(b)} = 0.2$ (dotted); $\gamma_{12}^{(b)} = 0.0$ (dash-dotted); and $\gamma_{12}^{(b)} = -0.2$ (solid). Results in **b** show the constant first spatial moment for the obstacles. Results in **c-d** show the second spatial moment of agents expressed in terms of $C_{11}(r)$ and $C_{12}(r)$, respectively. Both PCFs are given at $t = 60$. **d** The curves in red correspond to results from the spatial moment dynamics model, whereas curves in blue correspond to averaged data from the IBM. Parameter values are $p_1 = 1$, $d_1 = 0.5$, $m_1 = 5$, $p_2 = d_2 = m_2 = 0$, $\gamma_{11}^{(p)} = -0.38$, $\gamma_{12}^{(p)} = -0.38$, $\gamma_{21}^{(p)} = \gamma_{22}^{(p)} = 0$, $\gamma_{11}^{(b)} = 0.1$, $\gamma_{21}^{(b)} = \gamma_{22}^{(b)} = 0$, $\gamma_{11}^{(m)} = \gamma_{12}^{(m)} = \gamma_{21}^{(m)} = \gamma_{22}^{(m)} = 0$, $\sigma_{11}^{(p)} = 0.5$, $\sigma_{12}^{(p)} = 0.5$, $\sigma_{21}^{(p)} = 0.5$, $\sigma_{22}^{(p)} = 0.5$, $\sigma_{11}^{(b)} = 0.5$, $\sigma_{12}^{(b)} = 0.5$, $\sigma_{21}^{(b)} = 0.5$, $\sigma_{22}^{(b)} = 0.5$, $\sigma_{11}^{(m)} = 0.5$, $\sigma_{12}^{(m)} = 0.5$, $\sigma_{21}^{(m)} = 0.5$, $\sigma_{22}^{(m)} = 0.5$, $\mu_1^{(s)} = 0.4$, $\mu_2^{(s)} = 0.4$, $\sigma_1^{(s)} = 0.1$, $\sigma_2^{(s)} = 0.1$, $\sigma_1^{(d)} = 0.5$, and $\sigma_2^{(d)} = 0.5$.

bioRxiv preprint doi: https://doi.org/10.1101/267708; this version posted February 18, 2018. The copyright holder for this preprint (which was not certified by peer review) is the author/funder. All rights reserved. No reuse allowed without permission.



Results in Figure 7(a)-(d) show the spatial structure arising when there is a relatively strong repulsive bias between the obstacles and agents. This repulsion means that agents tend to move away from the obstacles, leading to the formation of a segregated spatial structure among agent-obstacle pairs. The corresponding auto-correlation and cross-correlation PCFs, given in Figure 8(c)-(d), are consistent with this as we see that $C_{12}(r) < 1$ over small distances. Here we note that the repulsive interactions between agents are sufficiently strong to counteract the short-range dispersal of agents. Hence we also observe a spatial segregation among agents over short distances. Results in Figure 7(e)-(h) and Figure 7(i)-(l) show a similar spatial pattern, but the effects are less pronounced due to the reduced repulsion. Results in Figure 7(m)-(p) are quite different since we have attraction between the agents and obstacles, and the agents are biased to move towards the obstacles. The attractive bias from obstacles is sufficiently large to counter the repulsive interaction between agents, leading to clustering of agents around obstacles.

Figure 8(a) shows the density dynamics of agents for each of the cases considered. The agent density decreases as the bias strength decreases and lowest when bias strength is negative. When the obstacle bias strength is negative corresponding to attractive obstacles, agents form clusters around obstacles. Since a large number of agents present at short distances, the proliferation rate of agents in clusters reduces significantly. Hence the population size increases more slowly than the case where obstacles are repulsive. Figure 8(b) shows the constant density of obstacles in each of the four cases.

## 6 Conclusion

In this work, we develop an IBM describing multi-species neighbor-dependent birth-death-movement processes, and we derive a continuum approximation of the stochastic dynamics using a spatial moment framework (Law et al. 2003; Plank and Law 2015; Binny et al. 2016a). Our modelling incorporates various processes such as neighbor-dependent directional bias from multiple subpopulations, and crowding effects such as contact inhibition of proliferation and contact inhibition of motility. We use this general framework to explore the case where one subpopulation is stationary and non-proliferative, and we treat this subpopulation as acting like biological obstacles in an *in vivo* environment. This framework allows us to explore how different properties of obstacles such as density, size and interaction strength influence the dynamics and emergence of spatial structure in the population.

Overall we see that the details of the dynamics of the population of agents and the spatial structure predicted using many identically prepared realizations of the IBM is reasonably well approximated by the numerical solution of the spatial moment model. Our results reveal some interesting features that are not obvious without careful consideration. For example, our results in Figure 3-4 show that as we increase the obstacle density, we observe that the steady state density of agents decreases, as we might expect. However, when

bioRxiv preprint doi: https://doi.org/10.1101/267708; this version posted February 18, 2018. The copyright holder for this preprint (which was not certified by peer review) is the author/funder. All rights reserved. No reuse allowed without permission.



we compare the accuracy of the spatial moments prediction, we see that the accuracy of the spatial moments model increases as the density of obstacles increases, which is not obvious. Overall, we see that the role of spatial patterns, such as clustering and segregation, is subtle. For example, results in Figure 3-4 shows that the long time steady arrangement of agents is segregated at short distances when there is a sufficiently low density of obstacles present. In contrast, we see a clustered arrangement of agents at short distances when there is a sufficiently large density of obstacles present. Without the kind of modelling framework that we present here these details are not at all obvious.

While our modelling framework is relatively general, there are many ways that our approach could be extended. For example, in this work we consider a spatially uniform initial distribution of agents and obstacles, and this kind of simulation is relevant to study relatively common cell biology experiments called a *proliferation assay*. However, other kinds of experiments, such as *scratch assays*, are initiated by considering an initial density of cells that varies spatially. To deal with this generalization, both the IBM and our analysis needs modification. Furthermore, throughout this study we always consider the influence of stationary obstacles. However, in some applications it is thought that mobile obstacles are more relevant (Wedemeier et al. 2009), and this could be dealt with by setting the obstacle motility rate to be positive. Another way that our work could be generalized is to consider different types of closure assumptions. While we obtain reasonable results using the power-2 closure scheme, it would also be of interest to consider other closure approximations (Murrell et al. 2004), or to consider extending the hierarchy of moment equations to deal with the dynamics of single agents, pairs of agents and triples of agents. Finally, while some recent progress has been made at calibrating single species IBM models to match experimental data (Browning et al. 2018), we are unaware of any attempts to calibrate multi-species IBMs to cell biology experiments. We leave these extensions for future consideration.

**Acknowledgements** This work is supported by the Australian Research Council (DP170100474). Computational resources are provided by the High Performance Computing and Research Support Group at QUT.

## References

1. Abramowitz M, Stegun IA (1972) Handbook of mathematical functions with formulas, graphs, and mathematical tables. Wiley, New York.
2. Bajenoff M, Egen JG, Koo LY, Laugier JP, Brau F, Glaichenhaus N, Germain RN (2006) Stromal cell networks regulate lymphocyte entry, migration, and territoriality in lymph nodes. Immunity 25(6): 989-1001.
3. Baker RE, Simpson MJ (2010) Correcting mean-field approximations for birth-death-movement processes. Phys Rev E 82: 041905.
4. Barraquand F, Murrell DJ (2013) Scaling up predator-prey dynamics using spatial moment equations. Methods Ecol Evol 4(3): 276-289.
5. Binny RN, Plank MJ, James A (2015) Spatial moment dynamics for collective cell movement incorporating a neighbour-dependent directional bias. J R Soc Interface 12(106): 20150228.

bioRxiv preprint doi: https://doi.org/10.1101/267708; this version posted February 18, 2018. The copyright holder for this preprint (which was not certified by peer review) is the author/funder. All rights reserved. No reuse allowed without permission.



6. Binny RN, Haridas P, James A, Law R, Simpson MJ, Plank MJ (2016a) Spatial structure arising from neighbour-dependent bias in collective cell movement. PeerJ 4: e1689.
7. Binny RN, James A, Plank MJ (2016b) Collective cell behaviour with neighbour-dependent proliferation, death and directional bias. Bull Math Biol 78(11): 2277-2301.
8. Bolker B, Pacala SW (1997) Using moment equations to understand stochastically driven spatial pattern formation in ecological systems. Theor Popul Biol 52(3): 179197.
9. Browning AP, McCue SW, Binny RN, Plank MJ, Shah ET, Simpson MJ (2018) Inferring parameters for a lattice-free model of cell migration and proliferation using experimental data. J Theor Biol. 437: 251-260.
10. Bruna M, Chapman SJ (2012) Excluded-volume effects in the diffusion of hard spheres. Phys Rev E 85: 011103.
11. Condeelis J, Segail JE (2003) Intravital imaging of cell movement in tumours. Nat Rev Cancer 3(12): 921-930.
12. Dyson L, Baker RE (2015) The importance of volume exclusion in modelling cellular migration. J. Math. Biol. 71(3): 691-711.
13. Edelstein-Keshet L (2005) Mathematical Models in Biology (Classics in Applied Mathematics). Society for Industrial and Applied Mathematics, New York.
14. Ellery AJ, Simpson MJ, McCue SW, Baker RE (2014) Characterizing transport through a crowded environment with different obstacle sizes. J Chem Phys 140: 054108.
15. Ellery AJ, Baker RE, McCue SW, Simpson MJ (2016) Modeling transport through an environment crowded by a mixture of obstacles of different shapes and sizes. Physica A 449: 74-84.
16. Finkelshtein D, Kondratiev Y, Kutoviy O (2009) Individual based model with competition in spatial ecology. SIAM J Math Anal 41(1): 297-317
17. Friedl P, Wolf K (2003) Tumour-cell invasion and migration: diversity and escape mechanisms. Nat Rev Cancer 3(5): 362-374.
18. Ghosh SK, Cherstvy AG, Grebenkov DS, Metzler R (2016) Anomalous, non-Gaussian tracer diffusion in crowded two-dimensional environments. New J Phys 18: 013027.
19. Gillespie DT (1977) Exact stochastic simulation of coupled chemical reactions. J Phys Chem 81: 2340-2361.
20. Hansen MM, Meijer LH, Spruijt E, Maas RJ, Rosquelles MV, Groen J, Heus HA, Huck WT (2016) Macromolecular crowding creates heterogeneous environments of gene expression in picolitre droplets. Nat Nanotechnol 11: 191-197.
21. Harley BA, Kim HD, Zaman MH, Yannas IV, Lauffenburger DA, Gibson LJ (2008) Microarchitecture of three-dimensional scaffolds influences cell migration behavior via junction interactions. Biophys J 95(8): 4013-4024.
22. Hasnain S, McClendon CL, Hsu MT, Jacobson MP, Bandyopadhyay P (2014) A new coarse-grained model for E. coli cytoplasm: accurate calculation of the diffusion coefficient of proteins and observation of anomalous diffusion. PLoS One 9(9): e106466.
23. Keller EF, Segel LA (1971) Model for chemotaxis. J Theor Biol 30: 225-234.
24. Kurosaka S, Kashina A (2008) Cell biology of embryonic migration. Birth Defects Res Part C: Embryo Today 84(2): 102122.
25. Law R, Dieckmann U (2000) A dynamical system for neighborhoods in plant communities. Ecology 81: 2137-2148.
26. Law R, Murrell DJ, Dieckmann U (2003) Population growth in space and time: Spatial logistic equations. Ecology 84: 252-262.
27. Le Clainche C, Carlier M (2008) Regulation of actin assembly associated with protrusion and adhesion in cell migration. Physiol Rev 88(2): 489-513.
28. Lewis MA (2000) Spread rate for a nonlinear stochastic invasion. J Math Biol 41: 430-454.
29. Martin P (1997) Wound healing-aiming for perfect skin regeneration. Science 276: 75-81.
30. Middleton AM, Fleck C, Grima R (2014). A continuum approximation to an off-lattice individual-cell based model of cell migration and adhesion. J Theor Biol. 359: 220-232.
31. Minton AP (2001) The influence of macromolecular crowding and macromolecular confinement on biochemical reactions in physiological media. J Biol Chem 276(14): 10577-10580.
32. Murray JD (1989) Mathematical biology. Springer, New York.
33. Murrell DJ, Dieckmann U, Law R (2004) On moment closures for population dynamics in continuous space. J Theor Biol 229: 421-432.

bioRxiv preprint doi: https://doi.org/10.1101/267708; this version posted February 18, 2018. The copyright holder for this preprint (which was not certified by peer review) is the author/funder. All rights reserved. No reuse allowed without permission.



34. Murrell DJ (2005) Local spatial structure and predator-prey dynamics: counterintuitive effects of prey enrichment. Am Nat 166: 354-367.
35. Ovaskainen O, Cornell SJ (2006) Asymptotically exact analysis of stochastic metapopulation dynamics with explicit spatial structure. Theor Popul Biol 69(1): 13-33.
36. Ovaskainen O, Finkelshtein D, Kutoviy O, Cornell SJ, Bolker B, Kondratiev Y (2014) A general mathematical framework for the analysis of spatiotemporal point processes. Theor Ecol 7(1): 101-113.
37. Plank MJ, Law R (2015) Spatial point processes and moment dynamics in the life sciences: A parsimonious derivation and some extensions. Bull Math Biol 77: 586-613.
38. Plank MJ, Simpson MJ (2012) Models of collective cell behaviour with crowding effects: comparing lattice based and lattice-free approaches. J R Soc Interface 9: 2983-2996.
39. Raghib M, Hill NA, Dieckmann U (2011) A multiscale maximum entropy moment closure for locally regulated space-time point process models of population dynamics. J Math Biol 62: 605-653.
40. Reverey JF, Jeon J, Bao H, Leippe M, Metzler R, Selhuber-Unkel C (2015) Superdiffusion dominates intracellular particle motion in the supercrowded cytoplasm of pathogenic Acanthamoeba castellanii. Sci Rep 5: 11690.
41. Shaw TJ, Martin P (2009) Wound repair at a glance. J Cell Sci 122: 3209-3213.
42. Shreshtha M, Surendran A, Ghosh A (2016) Estimation of mean first passage time for bursty gene expression. Phys Biol 13: 036004.
43. Simpson MJ, Binder BJ, Haridas P,Wood BK, Treloar KK, McElwain DLS, Baker RE (2013) Experimental and modelling investigation of monolayer development with clustering. Bull Math Biol 75: 871-889.
44. Simpson MJ, Plank MJ (2017) Simplified calculation of diffusivity for a lattice-based random walk with a single obstacle. Results in Physics 7: 3346-3348.
45. Smith S, Cianci C, Grima R (2017) Macromolecular crowding directs the motion of small molecules inside cells. J R Soc Interface 14: 20170047.
46. Sun M, Zaman MH (2017) Modeling, signaling and cytoskeleton dynamics: integrated modeling-experimental frameworks in cell migration. WIREs Syst Biol Med 9: e1365.
47. Tan C, Saurabh S, Bruchez MP, Schwartz R, LeDuc P (2013) Molecular crowding shapes gene expression in synthetic cellular nanosystems. Nat Nanotechnol 8: 602-608.
48. Tobin P, Bjornstad ON (2003) Spatial dynamics and cross-correlation in a transient predator-prey system. J Animal Ecology 72: 460-467.
49. Vedel S, Tay S, Johnston DM, Bruus H, Quake SR (2013) Migration of cells in a social context. Proc Natl Acad Sci USA 110: 129-134.
50. Warne DJ, Baker RE, Simpson MJ (2017) Optimal quantification of contact inhibition in cell populations. Biophys J 113: 1920-1924.
51. Wedemeier A, Merlitz H, Langowski J (2009) Anomalous diffusion in the presence of mobile obstacles. Europhys Lett 88: 38004.
52. Welch MD (2015) Cell migration, freshly squeezed. Cell 160: 581-582.
53. Zaman MH, Trapani LM, Sieminski AL, Mackellar D, Gong H, Kamm RD, Wells A, Lauffenburger DA, Matsudaira P (2006) Migration of tumor cells in 3D matrices is governed by matrix stiffness along with cell-matrix adhesion and proteolysis. Proc Natl Acad Sci USA 103: 10889-10894.